Consideration of Vacuum Vessel Properties Required for PFRC-type Fusion Reactors

Kim, Miles and Samuel Cohen

9/30/2021

Abstract

The fourth Princeton Field Reversed Configuration (PFRC-4) is a device designed to produce net power output through the fusion of deuterium and helium-3. Its inner walls would be bathed by 2.45 MeV neutrons as well as synchrotron and Bremsstrahlung radiation. The PFRC-4 device's vacuum vessel must serve several purposes including: shielding its magnets and any nearby human operators from neutron radiation; extracting useful energy from the incident radiation; and providing compatibility with RF heating. To find a suitable wall material, we report on nuclear, thermal, electrical, optical, and mechanical properties and fabrication techniques for the vessel. Neutron shielding, combined with weight and thickness requirements, strongly support the use of pure B-10 and its light compounds, e.g., boron carbide, and boron nitride. The variability of these properties with temperature and prolonged neutron exposure is described. We identify data not currently available for the materials considered. The dimensions of the vessel, the design of the cooling channels and how their geometry will affect thermal gradients and stresses in the vessel, and methods of manufacturing and assembling the vessel are also discussed. A multi-layer wall which separates the required functions is described.

1   Introduction

A field-reversed configuration (FRC) is a plasma configuration similar to a magnetic mirror, in that the plasma is in a cylindrical device, with a weak magnetic field where the bulk of the plasma exists, and a strong magnetic field at the exits of the configuration. This generally confines particles that are moving slow enough in the axial direction, but fails to confine faster particles in the direction parallel to the central axis. Unlike in a mirror configuration, an FRC is formed by an extremely strong azimuthal plasma current driven by an external source. The current is so strong, in fact, that it causes the field within it to switch directions and point in the opposite direction of the mirror field. This naturally causes a magnetic separatrix to form, resulting in a region where the magnetic field lines are closed, improving plasma confinement a great deal. The fourth Princeton Field-Reversed Configuration (PFRC-4) is a device that will use odd-parity rotating magnetic fields (RMF_O to drive this current while simultaneously heating the plasma to fusion-relevant temperatures through an induced electric field, producing a hot, dense plasma contained in an FRC core. This device will use deuterium (D) and helium-3 (He^3) as fuel for fusion, producing energy through the aneutronic fusion of the two elements. This reaction is only possible because of the incredibly high temperatures achievable in the core through this configuration, at least with respect to tokamak temperatures. However, because some D-D reactions will also inevitably take place, some neutrons will be produced. The PFRC-4 will use superconducting coils to act as flux conservers in the vessel, and these must be shielded from those neutrons to maintain an appropriate critical temperature so that they remain superconducting.

The PFRC-4 will need a vacuum vessel to serve three purposes in this process: neutron shielding, converting fusion energy released as radiation into electricity, and maintaining a vacuum within the FRC chamber.

2   Design Considerations

Designing a vacuum vessel to meet the three requirements mentioned above is no simple task. First, if it is to maintain a vacuum, the material chosen must be strong enough to endure the pressure stresses involved in such a venture. However, the vessel must also function as a neutron shield. To accomplish this, the chosen construction material will need to have either a high neutron absorption cross-section for high energy neutrons, or have a high neutron scattering cross-section followed by an outer layer of a different material with a high neutron absorption cross-section for low energy neutrons. Finally, the vessel must convert the fusion energy released as radiation into electricity, which involves two seperate processes. First, it must reflect synchrotron radiation back into the plasma to aid in heating it, and second, it must convert the Bremsstrahlung radiation into useful work. This will involve channels running throughout the vacuum vessel, lined with a material, such as tungsten, that will absorb the Bremsstrahlung radiation in the form of heat, which will be transferred to gaseous helium running through the channels. In order to allow the radiation to reach the channels, Bremsstrahlung radiation must not be reflected, but instead must be allowed to pass through the vessel until it reaches the tungsten-lined cooling channels. With these tasks in mind, the vacuum vessel must also be able to handle any thermal cycling, gradients, or other stresses involved in the operation of the fusion device, it must perform well under sustained neutron radiation, and must not shield the electric field induced by the RMF_O from the plasma within.

The PFRC-4 has two primary applications. It can be used as a spacecraft engine in the form of a Direct Fusion Drive (DFD), or it can be a small, portable power-plant for use in terrestrial applications. These two applications share some constraints, but they also each have unique requirements of their own.

2.1   Fusion Power Plant

The vacuum vessel for a terrestrial power plant does not need to be lightweight, and so mass is not a concern, other than for cost. Additionally, if the material of the vacuum vessel cannot maintain a vacuum, an exterior vacuum vessel can be used to provide vacuum to the entire system externally. This would be more costly, but the added mass at least would be unimportant. However, in this case, the vacuum vessel must shield neutrons not only from the superconducting coils, but also from human operators in the vicinity of the device. This may necessitate a very thick vacuum vessel for terrestrial applications.

One more thing that must be considered for a terrestrial power plant is its operational lifetime. When in operation, it is desirable that the parts for the device are long-lasting, so the plant can operate cost-effectively and produce continuous power for extended lengths of time. The requirements for the vacuum vessel of a power plant of

this sort was discussed in another study, and the necessary lifetime was assumed to be 30 years [1], and so in this study as well, the desired longevity for the vacuum vessel of a terrestrial power plant is considered to be 30 years.

2.2 Direct Fusion Drive

In the case of a DFD, the vacuum vessel must be as lightweight as possible, to maximize the specific impulse the engine can produce. However, the material used to produce the vacuum vessel need not be capable of holding a vacuum, since space holds a perfectly sufficient vacuum on its own. In addition, the engine need only shield neutrons form the superconducting coils, reducing the required thickness of the vessel.

The longevity needed for a DFD device is much lower than for the terrestrial application of the PFRC-4. In a previous study, a mission for a DFD-enabled spacecraft was discussed in detail, and the duration of that mission was 4 years [2]. As a result, this study will assume 4 years as the operational lifetime of DFD vacuum vessel as well.

3 Materials Considered

The first, most urgent step in designing the vacuum vessel for the PFRC-4 is to decide which material to construct it out of. This material must be an effective neutron shield, most likely by having a large nuclear absorption cross-section, and it must have a very low conductivity, or else it will cancel out the current induced by the RMF before it can reach the fusion plasma, thus wasting energy. The material must also be able to handle appreciable temperature ranges, gradients, and thermal cycling, while still having very specific optical properties due to the way it handles the various types of radiation emitted by the FRC core. The material needs to have sufficient mechanical strength so as not to get damaged during assembly and maintenance of the device, as well as to withstand thermal gradients. For aerospace applications, the material must also be lightweight and have a low emissivity, to avoid too much power loss to thermal radiation, while for terrestrial applications, it must be able to hold a vacuum, or else an additional apparatus will need to be designed to maintain the vacuum.

The first and second criteria mentioned pose the greatest difficulty and limit the choice of material greatly. There are a good number of materials that can shield out neutrons, but most of them have high conductivity. The only element that has an appreciable neutron absorption cross-section whilst not being a conductor is boron-10, the less common isotope of boron. As a result, a variety of compounds with high concentrations of boron are discussed, with primary goal of absorbing most of the 2.45 MeV neutrons that are released by the fusion reactions in the FRC core.

Another approach that is commonly used is to first "thermalize" the neutrons, or slow them down until they are in thermal equilibrium with the shielding material, by using a material with a high neutron scattering cross-section, lowering the energy of the neutrons from 2.45 MeV to a mere 0.025 eV. Then, a thin outer layer of a material with a high thermal neutron absorption cross-section is added to absorb the now slower and easier-to-capture neutrons. At lower neutron energies, neutron absorption cross-sections increase dramatically, allowing the absorbing layer to be fairly thin. For this reason, lithium hydride is also considered, since it is lightweight and contains hydrogen, which both has a high neutron scattering cross section and a very high energy absorption per scattering event in comparison to other elements. Naturally, lithium hydride must be accompanied by a thin outer layer of a boron-rich compound as well.

Due to these considerations, four compounds are considered in this study: elemental boron, boron carbide, boron nitride, and lithium hydride. A discussion of the phase diagrams and applicable crystal structures of each element is included in the following sections.

3.1 Elemental Boron

Elemental boron is composed purely of boron atoms. The phase diagram for elemental boron has been a matter of much contention among material scientists. However, experimental phase
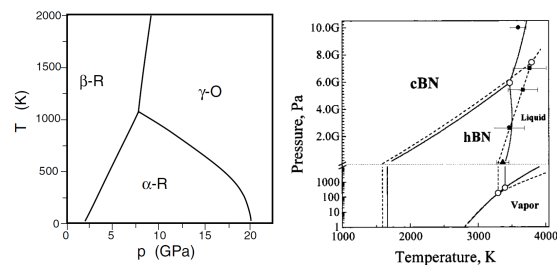
Figure 1: Phase Diagrams of (a) elemental boron [3] and (b) boron nitride [4].

diagrams for Boron have been experimentally compiled by a couple different groups, and one such diagram is given in Figure 1. It can be seen from this diagram that within a reasonable range of temperatures and pressures, boron is of the β-rhombohedral structure. However, α-rhombohedral boron is also practically stable within the temperature range that is relevant to the vacuum vessel, and can even be synthesized at low temperatures, though at large pressures, so this type of elemental boron could also be used [3]. However, all currently feasible manufacturing methods involve heating of the boron to high temperatures, at which point it transforms into β-rhombohedral boron, making α-rhombohedral boron an impractical choice for this application [6].

3.2   Boron Nitride

Boron nitride is composed of equal concentrations of boron and nitrogen, and has a variety of crystal structures, but at the pressures and temperatures the vacuum vessel will experience, it has two stable configurations, one of which is obvious from the phase diagram in Figure 1 [4], though hexagonal boron nitride is also practically stable[7]. In fact, hexagonal boron nitride is in wide use today and is the easier of the two to synthesize, and cubic boron nitride is more difficult to work with.

The hexagonal form of boron nitride is much softer than the cubic form, which is the hardest material besides diamond known to be in existence [7]. Both are considered in this study. Boron nitride has the disadvantage of having less than a 50% concentration by weight of boron due to nitrogen being heavier than boron, so it is the least desirable of the considered boron compounds in terms of weight, at least at first glance.

Figure 2: Phase Diagram of boron carbide with respect to **concentration** and temperature [5].

3.3   Boron Carbide

Boron carbide is composed of large amounts of boron, with small amounts of carbon included throughout its crystal structure. It has only one practically stable configuration of note, as can be seen from Figure 2 [5]. Though a range of concentrations of carbon can be introduced to boron carbide to enhance its qualities, since our goal is a high nuclear cross-section in the material, only stoichiometric boron carbide is considered in this study, to reduce carbon content in the mixture. Stoichiometric boron carbide is boron carbide that has the concentration indicated by its chemical formula, B_4C.

3.4   Borosilicate Glass

During this study, borosilicate glass is briefly discussed in one section. However, due to its very low concentration of boron, it proves to be an undesirable material, not to mention its low temperature tolerance. As a result, it is not considered further.

3.5   Lithium Hydride

Lithium hydride is composed of equal concentrations of lithium and hydrogen. It is a particularly good material to scatter and thermalize neutrons, because hydrogen atom has a high scattering cross-section and dissipates more energy per scattering event than any other element. It has only one crystal structure of note to this application, which in Figure 3 [8] is the β phase on the rightmost vertical axis, with a concentration indicated by the chemical formula

LiH. The α phase is simply pure lithium, which does not occur with the proper concentration of lithium hydride. As a result, only one phase need be considered.

It should be noted that lithium hydride can be made of deuterium or tritium instead of hydrogen. Such compounds are much more expensive and have inferior shielding capabilities. This will be demonstrated in subsubsection 4.1.2 for lithium deuteride, and lithium deuteride and lithium tritide are not considered anywhere else in this study.

4 Material Requirements

The goal in selecting a material for the PFRC-4 vacuum vessel is to choose a compound that has the specific properties the vessel requires. The difficulty is that the vacuum vessel requires so many specific properties, as described before. It needs to be lightweight, have electrical properties that do not cause shielding of the RMF_O coils, have optical properties that reflect some wavelengths and transmit others, have thermal and mechanical properties that allow it to withstand temperature gradients, and maintain these properties in the face of thermal cycling and neutron radiation. As a result, it is likely that no material will fit all of these criteria, and some creativity will need to be employed to construct a functional vessel. However, the first step is to simply find and list the properties of each material that pertain to each requirement of the vacuum vessel. This will be done in the following subsections.

Figure 3: Phase Diagram of lithium hydride with respect to **concentration** and temperature [8].

4.1 Mass Requirements and Economics

One of the most important factors in designing the vacuum vessel for a DFD engine is weight. It is vital when designing anything related to space travel that it be as light as possible, so that the spacecraft can move a further distance per unit fuel. An acceptable weight will be considered about 9000 kg [2], though in reality the vessel should be as light as possible. When designing a vacuum vessel for terrestrial applications, such as for a power plant, weight is of direct import, but ultimately impacts cost, which does matter and is strongly coupled with weight.

As a result, calculations must be done to determine the mass and ultimate cost of the vessel using each compound. This requires densities and unit costs ($/g) for each compound, as well as a calculation of the inner radius and thickness needed for the vacuum vessel, since this will determine the volume. These calculations and their ultimate impact on the total weight and cost of the vacuum vessel are given in this section.

4.1.1 Inner Radius Calculations

The primary consideration in determining the inner radius of the vacuum vessel is confinement. In the PFRC-4, there is a hot FRC core where fusion reactions occur and energy is released, and there is also a comparatively cool outer layer of plasma that flows through the chamber from one end of the device to the other around the FRC, extracting heat from it in the process. This stream of plasma is generated from a gas box and is then split into two streams by a flow-separating object at the base of the stream. The cool plasma is separated from the FRC core by a small gap to avoid contact, which would cause cooling in the core by the outer plasma. The core can be up to $r_c = 29$ cm in radius, and the gap thickness t_g and vacuum vessel inner radius r_i must be chosen so as to contain certain types of particles within the core while allowing others to escape and carry heat out of the core with them while still avoiding collision with the wall of the vessel. These considerations require an understanding of the nuclear reactions involved in the core, since these will determine the different particles present in the core and which ones should be allowed to escape. Another key element of this analysis is to avoid excessively high-energy neutron generation.
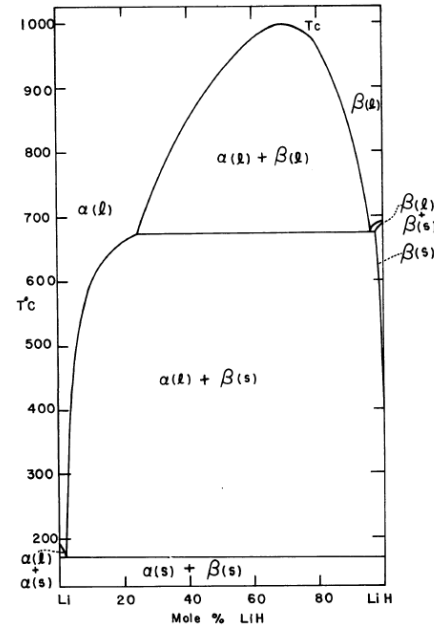
The PFRC-4 will ultimately be powered by an equal mix of deuterium (D), a stable isotope of hydrogen with one proton and one neutron, and helium-3 (He^3), a stable isotope of helium with two protons and one neutron. This is the primary nuclear reaction that will produce energy in the device, and is described by Equation 1.

$$D + He^3 \longrightarrow He^4(3.6\,\text{MeV}) + p(14.7\,\text{MeV}) \tag{1}$$

Because this reaction produces most of the power in the PFRC-4, it is important that D and He^3 particles are confined to the core. However, the helium-4 (He^4) and the proton (p) in the products should be allowed to leave the core, since they do not contribute to the production of fusion power. Additionally, because there are a significant number of D ions in the core, it is inevitable that some D-D reactions will occur. This reaction has two equally probable outcomes, which are described by Equation 2 and Equation 3.

$$D + D \xrightarrow{50\,\%} T(1.01\,\text{MeV}) + p(3.02\,\text{MeV}) \tag{2}$$
$$\xrightarrow{50\,\%} He^3(0.82\,\text{MeV}) + n(2.45\,\text{MeV}) \tag{3}$$
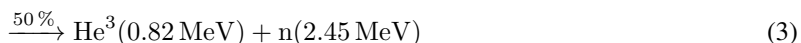
There are two new elements present in these reactions. First, there is a 2.45 MeV neutron, which is responsible for the bulk of the neutrons that need to be shielded by the vacuum vessel. However, neutrons have no impact on the dimensions of the vacuum vessel, since they cannot be confined in the first place due to their lack of charge. Second, there is a tritium (T) ion, which has one proton and two neutrons. This product happens to make a fourth fusion reaction possible. This reaction is described by Equation 4.

$$D + T \longrightarrow He^4(3.5\,\text{MeV}) + n(14.1\,\text{MeV}) \tag{4}$$

This reaction has no new products, but it produces a massively energetic neutron. In fact, it is an order of magnitude more energetic than the neutron produced in Equation 3, and so is much, much more difficult to either thermalize or absorb. Once the reaction occurs, shielding such neutrons is quite costly. As a result, T ions should be allowed to leave the core along with He^4 and p ions, in order to avoid this reaction.

In order to accomplish the confinement of D and He^3 ions to the core while simultaneously releasing p, R, and He^4 particles to the cold plasma outside of the core, t_g must be selected to be larger than the gyroradii of the confined particles, so they never come in contact with the stream, while being smaller than the gyroradii of all other fusion products. This is important, and though it is not actually relevant to deciding the inner radius of the vacuum vessel, it will be calculated for completeness. In addition, to avoid collisions of fusion products with the vacuum vessel wall, the inner radius of the vacuum vessel must be larger than the sum of r_c and the largest gyroradius of the released fusion products. The gyroradii of each particle have been calculated and are presented in Table 1. These values were calculated using the NRL Plasma Formulary [9], with the variables shown as they are defined there. The magnetic field within the device is about $B = 60,000$ G. It should be noted that not all products will try to leave the core head-on, but may approach the core edge at an angle. To account for this, the gyroradius of each particle at 45 degrees from the FRC axis is also calculated.

Particle	$T_\perp$ (MeV)	$T_{45°}$ (MeV)	μ	Z	r (cm)	$r_{45°}$ (cm)
e	0.050	0.025	-	-	0.01305	0.0094
D	0.10	0.05	2	1	0.76	0.54
He^3	0.10	0.05	3	2	0.47	0.33
He^3	0.82	0.41	3	2	1.33	0.94
He^4 (α particle)	3.60	1.80	4	2	3.23	2.28
p	14.70	7.35	1	1	6.52	4.61
T	1.01	0.505	3	1	2.96	2.09
p	3.02	1.51	1	1	2.95	2.09
He^4 (α particle)	3.50	1.75	4	2	3.18	2.25

Table 1: Gyroradius calculations for all particles involved in the PFRC, with the contained particles first, and the released particles last [9].

From this data, it is clear that $r_i > 35.52$ cm and 1.33 cm $< t_g < 2.088$ cm. The following values were chosen to make sure T is released and also to avoid particle-wall collisions:

$$t_g = 1.7 \text{ cm}$$
$$r_i = 35.6 \text{ cm}$$

4.1.2 Thickness, Weight, and Cost Calculations

With the inner diameter decided, the geometry of the vacuum vessel is fully defined except for its thickness. It is a cylindrical shell of inner radius $r_i = 35.6$ cm and length $l = 500$ cm, with an approximately cylindrical fusion core of radius $r_c = 29$ cm and elongation $e = 5$. The thickness is limited by the amount of neutron radiation acceptable to the superconducting flux-conservers that surround the vacuum vessel. A previous project report [1] by Walsh and Griffin reported a total fluence of 6.00×10^{17} neutrons per square centimeter as the maximum allowable fluence, and this value is adopted here.

In order to find the thickness needed for both the space and terrestrial lifetimes set previously, the geometry above described was set up in a open-source Monte Carlo simulation code called OpenMC [10]. Then, the FRC core was considered to be producing 6.11413×10^{16} neutrons each second, evenly distributed across the cylindrical space of the core, as set forth by Walsh and Griffin. The fluence at the outer surface of the vessel was then recorded for each of a large number of trials with different material layers of different thicknesses, and used to calculated the maximum lifetime of the configuration. First, this method was used to reproduce the results achieved for boron carbide by Walsh and Griffin, and then a large number of possible material combinations were tested using it. The process was repeated for each option until the desired lifetime for the application in question was critically achieved. Densities and unit prices for each of the compounds have been gathered as well, and used to calculate weights and costs for each material configuration. These costs are very rough, as the market for these materials will likely change by the time the PFRC-4 is constructed, and the costs displayed are based only on scaled powder costs, excluding manufacturing costs. Both terrestrial and space applications are considered, and the data is displayed in Table 2. As will be the case in all tables with colored cells, favorable outcomes are shaded green, unfavorable ones are shaded red, and acceptably unfavorable ones are shaded blue. Darker colors indicate an emphasized condition, with darker blue indicating more unfavorable options.

	B				hBN			
Density (g/cc)	2.35 [11]				2.10 [7]			
	Natural		Enriched		Natural		Enriched	
Unit Cost ($/g)	29.82 [12]		33.00 [13]		1.80 [12]		N/A	
	DFD		Terrestrial		DFD		Terrestrial	
	Natural	Enriched	Natural	Enriched	Natural	Enriched	Natural	Enriched
Thickness (cm)	32.75	23.90	42.70	32.50	45.75	37.00	49.70	49.60
Mass (kg)	12567	8390	17953	12441	17649	13206	19821	19765
Cost ($)	374.74	276.87	535.36	410.55	31.77	N/A	35.68	N/A

	cBN				B4C			
Density (g/cc)	3.48 [14]				2.55 [7]			
	Natural		Enriched		Natural		Enriched	
Unit Cost ($/g)	3.25 [15]		N/A		1.65 [12]		N/A	
	DFD		Terrestrial		DFD		Terrestrial	
	Natural	Enriched	Natural	Enriched	Natural	Enriched	Natural	Enriched
Thickness (cm)	37.00	29.40	49.60	38.20	31.50	24.30	40.80	32.80
Mass (kg)	21884	16168	32753	22844	12958	9295	18304	13664
Cost ($)	71.12	N/A	106.4	N/A	21.38	N/A	30.20	N/A

	LiH with 2cm hBN Layer				50% LiH, 50% B Powder Mixture			
Density (g/cc)	0.78 [8]				1.57			
	Natural		Enriched		Natural		Enriched	
Unit Cost ($/g)	0.54 [13]		N/A		17.41		19.42	
	DFD		Terrestrial		DFD		Terrestrial	
	Natural	Enriched	Natural	Enriched	Natural	Enriched	Natural	Enriched
Thickness (cm)	24.50	23.60	32.80	32.00	27.50	24.40	36.20	32.60
Mass (kg)	3679	3535	5095	4951	6672	5734	9558	8319
Cost ($)	3.01	N/A	3.91	N/A	116.20	106.78	166.44	154.90

	50% LiH, 50% hBN Powder Mixture				50% LiH, 50% hBN, 2cm hBN Layer			
Density (g/cc)	1.49				1.49			
	Natural		Enriched		Natural		Enriched	
Unit Cost ($/g)	1.49		N/A		1.49		N/A	
	DFD		Terrestrial		DFD		Terrestrial	
	Natural	Enriched	Natural	Enriched	Natural	Enriched	Natural	Enriched
Thickness (cm)	31.40	29.60	41.40	39.60	29.75	27.50	39.70	37.50
Mass (kg)	7548	6990	10921	10280	7912	7205	11322	10528
Cost ($)	11.28	N/A	16.33	N/A	12.09	N/A	17.23	N/A

	LiD with 2cm hBN Layer				50% LiD, 50% B Powder Mixture			
Density (g/cc)	0.88 [8]				1.62			
	Natural		Enriched		Natural		Enriched	
Unit Cost ($/g)	39.20 [13]		N/A		34.07		N/A	
	DFD		Terrestrial		DFD		Terrestrial	
	Natural	Enriched	Natural	Enriched	Natural	Enriched	Natural	Enriched
Thickness (cm)	35.00	30.80	46.75	41.70	31.40	25.60	41.10	34.50
Mass (kg)	6100	5247	8748	7563	8180	6292	11720	9260
Cost ($)	203.8	N/A	301.79	N/A	278.7	N/A	399.3	N/A

Table 2: Mass and cost calculations for each material. Note that the costs cited are for purchasing the powder alone, and do not include possible manufacturing costs.

A quick look at the data leads to a quick dismissal of cubic boron nitride and lithium deuteride. When it comes to weight, β-rhombohedral boron and hexagonal boron nitride are the best absorption options, while configurations containing lithium hydride are all even lighter than these. However, when it comes to cost, boron carbide appears to be the most cost-effective absorption material, followed by hexagonal boron nitride, while β-rhombohedral boron is exorbitantly expensive. However, as before, lithium hydride is even cheaper still. Note that costs could not be readily gathered for enriched forms of the boron-rich compounds. However, they are likely to be both much more expensive and much lighter in the long run, due to the decrease in required thickness.

It seems that lithium hydride alone with a layer of hexagonal boron nitride would be a fantastic option, as far as weight and cost go. For its electrical properties however, a mixture could be better, which is why mixtures of lithium hydride with β-rhombohedral boron and hexagonal boron nitride are considered. Even as a mixture, lithium hydride options are still more desirable than others from the perspective of weight and cost. At this juncture, the cost of the vacuum vessel is of little import, but were the PFRC-4 to be commercialized, cost would become a key factor.

4.2 Electrical Requirements

The PFRC-4 device heats the FRC core to fusion-relevant temperatures using an odd-parity rotating magnetic field (RMF_O). This RMF_O produces an induced electric field that drives the plasma current. However, if any conductive material exists between the RMF_O and the plasma, a current will be induced in it which will siphon off power to resistive heating in the vacuum vessel that was intended to have heated the plasma. To minimize these losses, the vacuum vessel must be made of a material that has limited conductivity, or high resistivity.

The RMF_O in the PFRC-4 will have a frequency of $f_R = 0.5$ MHz, which results in an angular frequency of $\omega_R = 3.14 \times 10^6$ and a magnitude of $B_R = 6 \times 10^{-3}$ T, which is much smaller than the mirror field generated by the sollenoidal coils. Now, invoking Faraday's law in Equation 5 and assuming that $\left| \frac{d\vec{B}}{dt} \right| \approx \omega_R B_R$ and $\left| \nabla \times \vec{E} \right| \approx \frac{E}{r}$, Equation 6 results.

$$\nabla \times \vec{E} = -\frac{d\vec{B}}{dt} \tag{5}$$

$$\implies E = -\omega_R B_R r \tag{6}$$

Invoking Ohm's law, an expression for current density (Equation 7) and an expression for voltage result (Equation 8).

$$\vec{j} = \sigma \vec{E} = 1.885 \times 10^4 r \sigma \tag{7}$$

$$\Delta V = 2\pi r E = 1.184 \times 10^5 r^2 \tag{8}$$

Power dissipated is then found by integrating, as in Equation 9. For the sake of this calculation, the vessel is considered to be 20 cm thick.

$$P = \int_{r_i}^{r_o} j \cdot \Delta V L \, dr = \int_{r_i}^{r_o} 1.116 \times 10^{10} \sigma r^3 \, dr = 2.790 \times 10^9 \sigma (r_o^4 - r_i^4) = 2.219 \times 10^8 \sigma \tag{9}$$

The power being transferred to the plasma ideally by the RMF_O is 110 kW, and to keep power losses low, this study assumes a power loss of up to 1%, or 1.1 kW, to be acceptable. With this information, the maximum conductivity σ tolerable, or the minimum resistivity $\rho = \frac{1}{\sigma}$ tolerable, is calculated in Equation 11 and Equation 12.

$$2.134 \times 10^8 \sigma = 1100 \tag{10}$$

$$\implies \sigma_{\text{max}} = 4.96 \times 10^{-8} \ \Omega^{-1} \cdot \text{cm}^{-1} \tag{11}$$

$$\implies \rho_{\text{min}} = \frac{1}{\sigma_{\text{max}}} = 2.02 \times 10^7 \ \Omega \cdot \text{cm} \tag{12}$$

Any material that violates these values will cause a loss greater than 1% of the RMF_O power, which is undesirable. Conductivities and resistivities were gathered for each of the considered materials, and are displayed in Table 3. Data was gathered at room temperature and also at a high temperature of 800 K, and colored cells follow the same rules as previously outlined.

Property	β-B	hBN	cBN	B_4C	LiH
At Room Temperature					
σ ($\Omega^{-1}cm^{-1}$)	8.58×10^{-8} [16]	1.00×10^{-12} [7]	1.00×10^{-10} [17]	5.84×10^{-3} [18]	3.16×10^{-8} [19]
ρ ($\Omega^1 cm^1$)	1.17×10^7 [16]	1.00×10^{12} [7]	1.00×10^{10} [17]	1.71×10^2 [18]	3.16×10^7 [19]
At 800 K					
σ ($\Omega^{-1}cm^{-1}$)	1.00 [16]	5.00×10^{-10} [20]	1.00×10^{-7} [17]	2.89×10^1 [21]	2.15×10^{-4} [13]
ρ ($\Omega^1 cm^1$)	1.00 [16]	2.00×10^9 [20]	1.00×10^7 [17]	3.46×10^{-2} [21]	4.64×10^3 [13]

Table 3: Cited values of electrical properties at two different temperatures.

From this data, it is clear that, as far as conductivity goes, boron carbide is not a good choice. In fact, these values for boron carbide are not even the highest values of conductivity possible for the material [22]. Additionally, β-rhombohedral boron also appears to be a poor choice in terms of conductivity, especially at high temperatures. Cubic boron nitride is a feasible choice, but does not quite meet the standard set at high temperatures. The best choice, conductivity-wise, is hexagonal boron nitride. Hexagonal boron nitride will not shield out much of the power from the RMF_O, even at high temperatures. Lithium hydride also gets close to being acceptable, but ultimately it would dissipate 43 percent of the RMF_O power, which is a lot higher than desired.

4.3   Optical Requirements

A large amount of the energy being generated in the PFRC-4 will be released in the form of Bremsstrahlung and synchrotron radiation. Currently, the vacuum vessel is meant to deal with these two forms of energy in different ways. The Bremsstrahlung radiation is to be allowed to pass through the vessel until it reaches and is absorbed by tungsten lining in the channels which will be built into the vacuum vessel, and thus be converted to heat and transported to a heat engine process external to the vessel. In contrast, the synchrotron radiation is to be reflected off of the inner wall of the vacuum vessel, so that such energy will be returned to the fusion plasma to aid heating it.

As a result of these requirements, it is important that the material used to construct the vacuum vessel have the correct optical properties in the frequency ranges of the Bremsstrahlung and synchrotron radiation, respectively. Though we would prefer no energy loss, in this study it will be considered acceptable if only 10 percent of the energy incident on the vacuum vessel and parallel to its inner surface does not go to the desired source. Thus, the reflectivity of the material must be at most 0.1 when in the frequency range of the Bremsstrahlung radiation, which is in the x-ray range of around $f_{brem} = 10^{18}$Hz. Likewise, the reflectivity of the material must be at least 0.9 in the frequency range of the synchrotron radiation, which is around $f_{ce} = 2.80 \times 10^6 B = 1.68 \times 10^{11}$Hz, with the magnetic field being $B = 60,000$ G, as defined before.

In order to determine the reflectivity of each material in this range, data was gathered from a variety of sources on each. The data gathered from these sources came in a variety of forms, including indices of refraction, which were converted to reflectivities using Equation 13, which comes from a trusted optics textbook [23].

$$R = \left(\frac{\tilde{n} - 1}{\tilde{n} + 1}\right)\left(\frac{\tilde{n} - 1}{\tilde{n} + 1}\right)^* = \frac{(n_R - 1)^2 + n_l^2}{(n_R + 1)^2 + n_l^2} \tag{13}$$

$$\tilde{n} = n_R - \mathbf{i} \cdot n_l \tag{14}$$

4.3.1   Elemental Boron

Most of the data available for elemental boron was for β-rhombohedral boron, but thin films were used to take some of the data. Figure 4 shows the reflectivity data collected for elemental boron.
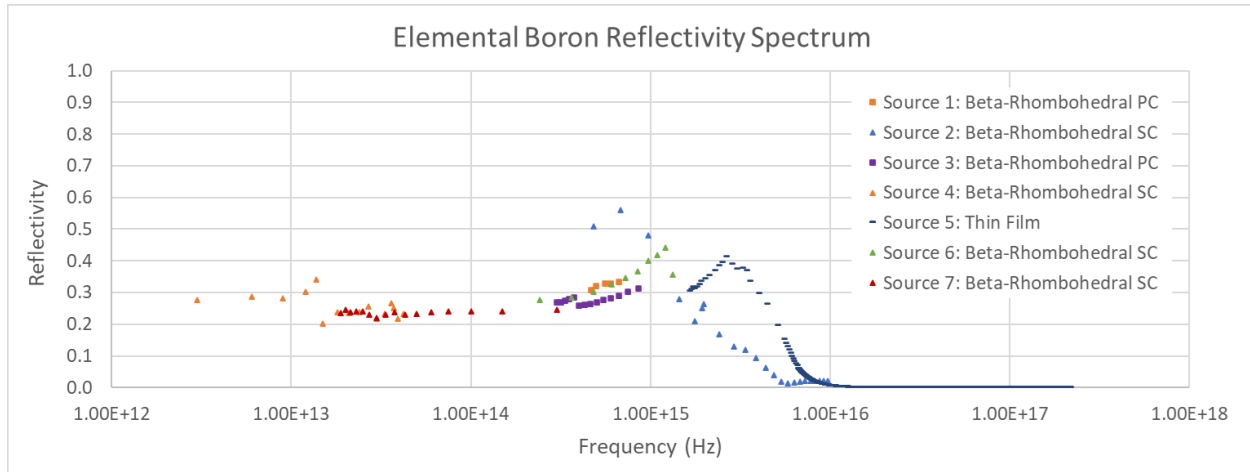
Figure 4: Reflectivity as a function of wavelength for beta-rhombohedral boron. Sources 1 [24], 2 [25], 3 [26], 4 [27], 5 [28], 6 [29], and 7 [30] are listed in the bibliography.

No data is available within either of the desired frequency ranges specified, as can be seen in Figure 4. Thus, this data must be acquired through additional testing.

4.3.2 Boron Nitride

Because boron nitride comes in two distinctive structures, data was gathered separately for both structures.

4.3.2.1 Hexagonal Boron Nitride   Hexagonal boron nitride was mainly tested using thin films, not bulk samples. Figure 5 shows the compiled data.
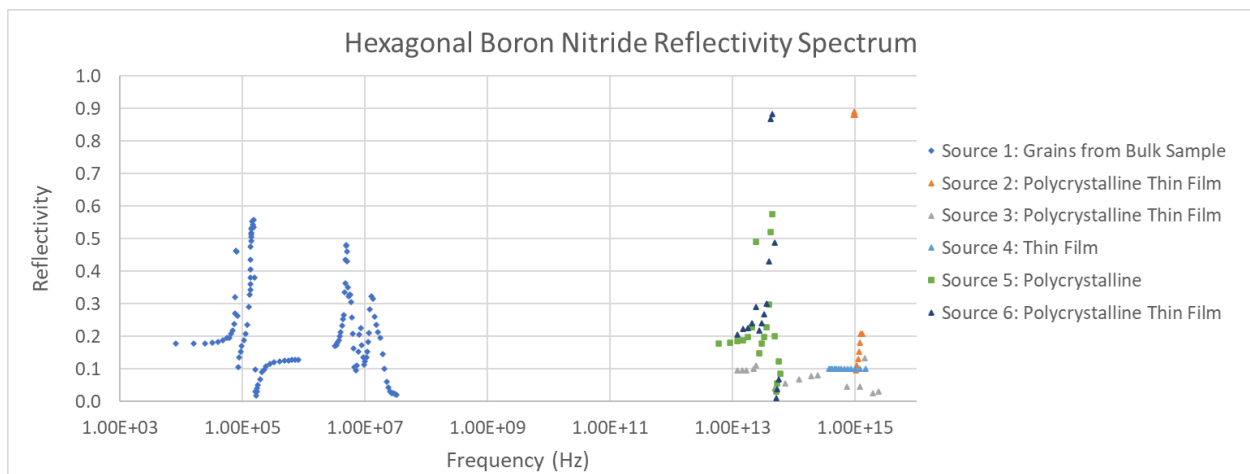
Figure 5: Reflectivity as a function of frequency for hexagonal boron nitride. Sources 1 [31], 2 [32], 3 [33], 4 [34], 5 [35], and 6 [36] are listed in the bibliography.

As with β-rhombohedral boron, there is still no information in the two ranges of importance specified above. As a result, hexagonal boron nitride must also be tested for further reflectivity data.

4.3.2.2 Cubic Boron Nitride   Cubic boron nitride, unlike its hexagonal counterpart, was mainly tested for reflectivity using single-crystal samples. The results are shown in Figure 6.

11
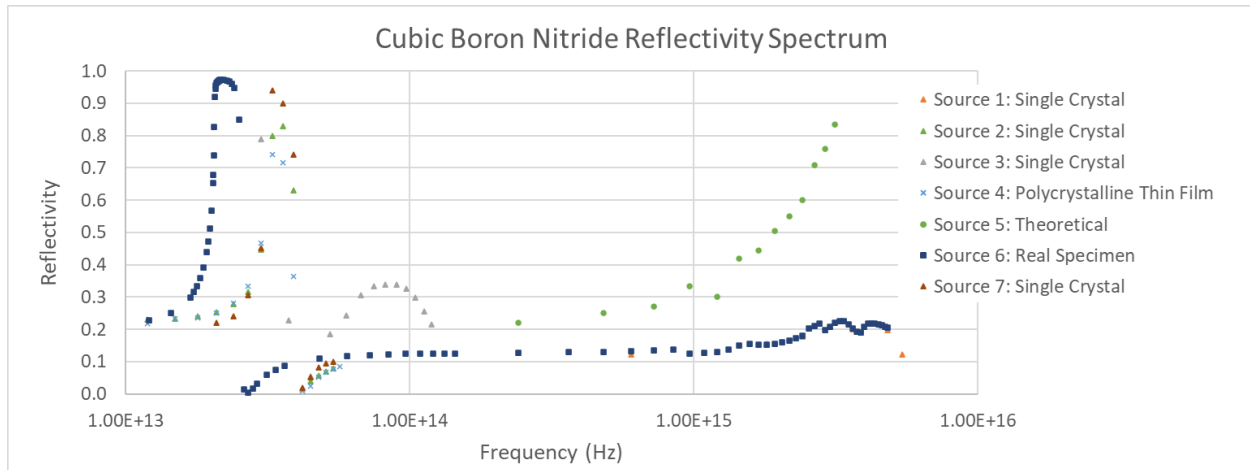
Figure 6: Reflectivity as a function of frequency for boron carbide. Sources 1 [37], 2 [38], 3 [39], 4 [36], 5 [40], 6 [41], and 7 [42] are listed in the bibliography.

As with hBN, no reflectivity data is available for the synchrotron and Bremsstrahlung frequency ranges, once more revealing the need for further tests.

It should be noted that hBN and cBN have very similar reflectivity curves, a fact that becomes clear when their data is combined into a single plot, as in Figure 7. As a result, it is possible that cubic and hexagonal boron nitride do not both need to be tested, which would be very beneficial considering how difficult it is to obtain cubic boron nitride in bulk form.
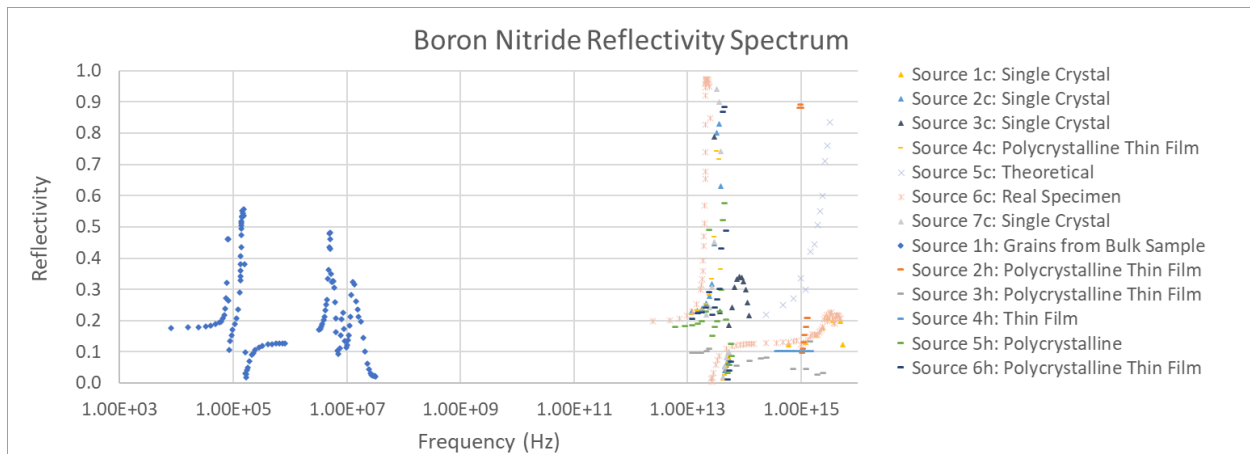
Figure 7: Reflectivity as a function of frequency for boron nitride. Sources 1c [37], 2c [38], 3c [39], 4c [36], 5c [40], 6c [41], 7c [42], 1h [31], 2h [32], 3h [33], 4h [34], 5h [35], and 6h [36] are listed in the bibliography.

4.3.3 Boron Carbide

Boron carbide reflectivity data was only available from thin film studies, similar to hexagonal boron nitride. The compiled data is displayed in Figure 8.
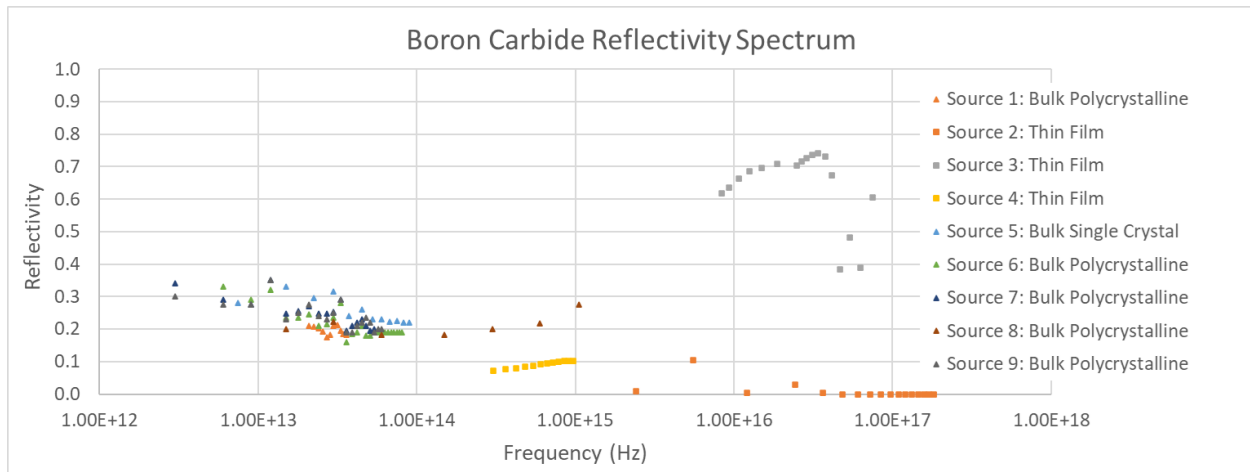
Figure 8: Reflectivity as a function of frequency for boron carbide. Sources 1 [43], 2 [44], 3 [45], 4 [46], 5 [47], 6 [48], 7 [49], 8 [50], and 9 [51] are listed in the bibliography.

As with the other compounds, Figure 8 has no data in the desired frequency ranges.

4.3.4 Lithium Hydride

Lithium hydride data is not readily available, but some sources were found. The data that could be found is displayed in Figure 9.
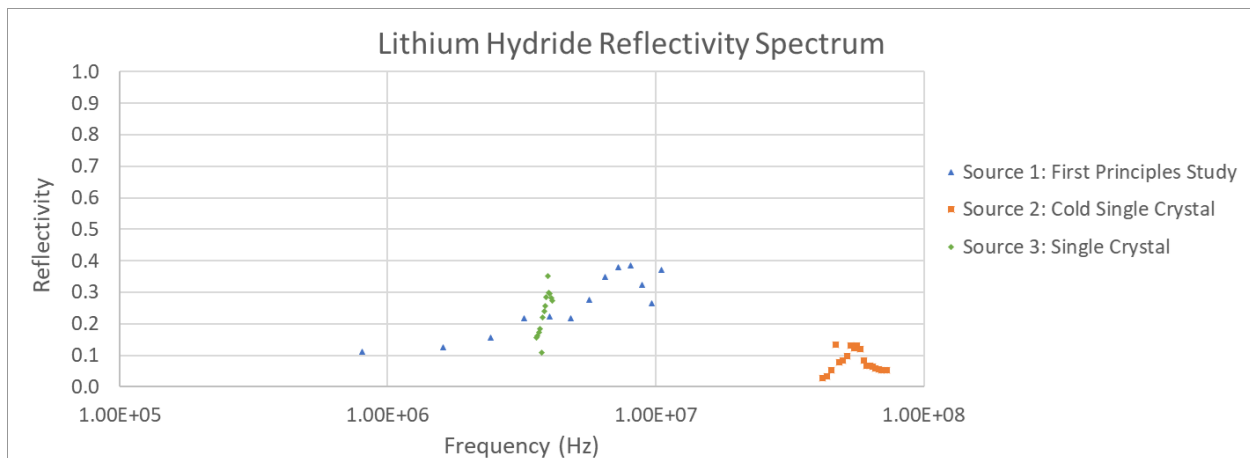
Figure 9: Reflectivity as a function of frequency for lithium hydride. Sources 1 [52], 2 [53], and 3 [54] are listed in the bibliography.

Figure 9 has no data in the desired frequency ranges at all, similar to the other compounds for which data was gathered. Ultimately, all five compounds require further testing to determine reflectivity in the proper frequency ranges.

4.4 Thermal Requirements

The vacuum vessel will also need to have cooling capabilities, as mentioned previously. To accomplish this, it will either need to have cooling channels running through it, or it will need to have cooling channels on the surface somewhere, to absorb heat produced by synchrotron and Bremsstrahlung radiation. However, such methods will require careful analysis to determine to what degree thermal gradients will form, and what types of stresses these

13

will impose on the material. Additionally, pressure will be exerted on the walls of the channels by the gaseous helium passing through them, causing additional stresses. An analysis of such stresses can be executed in Solidworks. However, to accomplish this analysis, some thermal properties of the considered materials are crucial. Specifically, the thermal conductivity, emissivity, coefficient of expansion, and specific heat of each material is of crucial importance. These gathered values are displayed in Table 4.

	β-B	B$_4$C	hBN	cBN	LiH
Upper Functional Temperature (K)	1226.00 [12]	900.00 [12]	1250.00 [12]	1200.00 [55]	800.00 [56]
At Room Temperature					
Conductivity (W m-1 K-1)	23.10 [57]	60.00 [12]	32.00 [58]	371.67 [59]	12.50 [8]
Emissivity	0.87 [60]	0.75 [60]	0.85 [60]	0.85 [60]	?
Expansion Coefficient (1e-6 K)	3.00 [61]	5.60 [12]	3.00 [58]	4.80 [55]	42.00 [8]
Specific Heat (J/kg*C)	1017 [62]	1000 [63]	665 [64]	786 [64]	4213 [8]
At 800 K					
Conductivity (W m-1 K-1)	11.50 [57]	36.00 [55]	57.45 [65]	265.00 [59]	4.00 [8]
Emissivity	0.83 [60]	0.75 [60]	0.73 [60]	0.73 [60]	?
Expansion Coefficient (1e-6 K)	5.00 [61]	5.60 [12]	1.78 [58]	4.80 [17]	61.00 [8]
Specific Heat (J/kg*C)	2127 [62]	1930 [66]	1588 [64]	1668 [64]	6936 [8]

Table 4: Cited values of thermal properties at two different temperatures.

In general, it seems that hexagonal boron nitride and boron carbide are likely to fare well with thermal gradients due to their somewhat low expansion coefficients and high conductivities. Boron carbide could also do well, considering its high specific heat, and thus its ability to take in a lot of heat without great changes in temperature. However, nothing is certain until simulations in Solidworks are executed.

The PFRC-4 will likely need to be shut down occasionally to undergo maintenance, upgrades, or configuration for testing. Each time the device is powered off, the vacuum vessel will need to be lowered to room temperature. This is not a factor when it comes to a space mission, but for terrestrial applications, it is of critical importance. As a result, each material must be investigated to see how it functions under thermal cycling as well.

4.4.1 Thermal Cycling

The vacuum vessel will be heated to the operating temperatures it is designed for, and then will be cooled automatically when maintenance must be done, before being heated once more. If this were to occur yearly or even every four years, it would result in a considerable amount of thermal cycling for the vacuum vessel. As a result, the response of each candidate compound to thermal shocks and cycles is quite important in the selection of a material for constructing the vacuum vessel.

4.4.1.1 β-Rhombohedral Boron Boron   Pure β-rhombohedral boron, and elemental boron in general, is very sensitive to thermal shocks. It is so sensitive, in fact, that it often cracks even after being formed at a high temperature and then being cooled quite slowly to room temperature [67]. As a result, pure β-rhombohedral boron appears to be a poor choice for terrestrial applications, though it is possible that further testing will prove otherwise.

4.4.1.2 Hexagonal Boron Nitride   Boron nitride in its hexagonal form is actually very promising as far as thermal cycling goes. One study showed that, as a result of the minimal grain growth that occurs within it even at temperatures approaching 2500 °C, boron nitride fibers are practically unaffected by thermal cycling. There was some confusion from this source about what the fibers were made of, but it was decided that they were likely hexagonal boron nitride fibers [68]. Though this is not conclusive, many non-academic sources, namely suppliers of boron nitride, claim that the material has a strong resistance to damage due to thermal cycling [69] [70].

The available data for hexagonal boron nitride suggests that it will function perfectly well under the thermal cycling loads it is likely to undergo. However, to know for certain, this must be verified through experiments.

4.4.1.3 Cubic Boron Nitride Cubic boron nitride is slightly less characterized than even hexagonal boron nitride when it comes to thermal cycling. However, one study does suggest that at temperature differences of greater than 300 K, the mechanical strength of the compound decreases dramatically [71]. As a result, unless it is decided that the Brayton cycle should function on such a low temperature difference, cubic boron nitride is likely not a good choice for terrestrial applications. However, more testing should be executed before a decision is made about the material with regards to the vacuum vessel.

4.4.1.4 Boron Carbide Boron carbide is characterized well when it comes to thermal cycling in tokamaks, as a coating. It has been repeatedly demonstrated that, when coating the wall of a tokamak, boron carbide can withstand high-temperature thermal cycling below 2000°C, and also at lower temperatures around 300 °C [72] [73] [74]. However, boron carbide is less well-tested when it comes to bulk samples. One study on sintered powder samples, which is much closer to how the PFRC-4 vacuum vessel will be manufactured, showed that it can withstand thermal cycling to around 700 °C without significant deterioration of mechanical properties. Further testing, however, would certainly be necessary before applying boron carbide to the construction of the vacuum vessel [75].

4.4.1.5 Lithium Hydride Lithium hydride has a large coefficient of thermal expansion, as listed previously, and this results in large voids and cracks appearing in it when it is cast. These move about within the material when it is thermal cycled, at least at temperatures approaching 800 K [76]. In fact, lithium hydride has been known to crack when repeatedly cycled to temperatures close to 600 °C, showing unquestionably disastrous cracking after 36 cycles [77].

This data suggests that lithium hydride is a poor choice when it comes to thermal cycling, though it has also mainly been tested at temperatures higher than the vacuum vessel will require. As a result, further testing ought to be carried out to ascertain just how much thermal cycling lithium hydride can withstand under the conditions the vacuum vessel will be exposed to.

Of the materials presented above, hexagonal boron nitride and boron carbide appear best suited to withstanding thermal cycling. However, additional testing is required for each compound before their performance in the specific case of the vacuum vessel can be determined. Additionally, none of the sources gathered speak of the impact of thermal cycling on electrical, thermal, or optical properties, so this should also be investigated through further testing.

4.5 Mechanical Requirements

To complete the analysis in Solidworks mentioned in the previous section, some mechanical properties will also be required. These properties are the elastic modulus, tensile strength, and compressive strength of each material. With these, Solidworks will be able to complete the analysis, calculating mass and heat flows, temperatures, thermal expansion effects, pressure effects, and ultimately stresses throughout the device. The necessary properties are listed in Table 5.

	β-B	B_4C	hBN	cBN	LiH
Elastic Modulus (Gpa)	441 [12]	440 [12]	61 [58]	71 [55]	136 [52]
Tensile Strength (Mpa)	1580 [12]	469 [78]	80 [58]	48 [55]	13 [79]
Compressive Strength (Mpa)	345 [67]	2800 [12]	165 [12]	175 [55]	101 [80]
Endurance Limit (Mpa)	?	222 [7]	?	?	?

Table 5: Cited values of mechanical properties of considered compounds.

It should be noted from this table that the endurance limit, or the stress above which repeated loading and unloading would cause eventual fracture, is only available for boron carbide. This value is simply listed because it could give some insight as to whether this material will be able to handle the thermal cycling imposed upon it by the conditions of the vessel.

15

In terms of mechanical strength, it is clear that pure boron is best in tension, while boron carbide is best in compression. Lithium hydride is somewhat weak, and this should be considered when choosing the method of construction for the vessel.

4.6 Neutron Damage Considerations

In general, a boron-10 atom splits into one lithium and one helium atom when a neutron is absorbed by the vacuum vessel, due to the massive comparative neutron absorption cross-section of boron-10. The lithium has a very minimal effect on the structure of the material when this occurs, but the helium atoms tend to gather into bubbles in the material and cause swelling, expansion, and ultimately cracking due to voids, even though a portion of the helium does diffuse out of the boron compound over time. In addition to this, every time a fast neutron is scattered through collisions with the vacuum vessel, atoms can be dispalced and ultimately cause voids, dislocations, and swelling to occur as well, and this effect impacts lithium hydride as well, despite its lack of boron content [**?**]. These mechanisms damage the crystal structure of the vessel, altering its properties and possibly rendering it unfit for use. Each material responds differently to the damage, with some more durable to it than others, and so these effects must be considered in the selection of a material for the vacuum vessel.

It should be noted that most materials are not well-characterized when it comes to properties as a function of neutron fluence. This is partially because the shielding or absorption of neutrons is done in such niche applications that each application requires a different set of tests and data. However, most will provide information in the way of maximum allowable neutron fluence. As a result, the maximum neutron fluence in the vacuum vessel over a course of both 4 and 30 years is calculated in Equation 15 and Equation 16 at the inner wall, where fluence will always be greatest.

$$f_{max,DFD} = \frac{6.11413 \times 10^{16}}{2\pi r_i L} \cdot 3.15 \times 10^7 \cdot 4 = 6.89 \times 10^{19} \text{ n/cm}^2 \tag{15}$$

$$f_{max,terr} = \frac{6.11413 \times 10^{16}}{2\pi r_i L} \cdot 3.15 \times 10^7 \cdot 30 = 5.17 \times 10^{20} \text{ n/cm}^2 \tag{16}$$

These fluences must be manageable by the material, or there will be unacceptable damage to the vacuum vessel in the time periods described, starting on the plasma-facing surface.

4.6.0.1 β-Rhombohedral Boron β-rhombohedral boron is not well characterized, for it is not frequently used directly in structural or nuclear applications. Often, boron carbide or boron nitride are used in applications where the neutron absorption properties of boron are necessary, such as in nuclear fission reactors. Most of the time the structural properties are not as important in such applications as with a vacuum vessel, and the boron compounds are often simply packed as powder into steel casings. However, since elemental boron struggles so much with thermal shocks and has such a higher percentage of boron-10 atoms than its fellow compounds, it will likely fare poorly, and show mechanical weakness and failure rapidly under sustained neutron radiation. However, this property will need to be tested further if β-rhombohedral boron is to be considered for vacuum vessel design.

4.6.0.2 Hexagonal Boron Nitride Hexagonal boron nitride is somewhat more characterized than elemental boron, due to its common use in fission reactors. One study shows that hexagonal boron nitride can withstand a fluence of 5.75×10^{16} neutrons per square centimeter while swelling only 4.5 percent [81]. Unfortunately, that is far too low of a fluence for either application of the vacuum vessel, by four orders of magnitude. Similarly, the electrical properties of hexagonal boron nitride were shown to deteriorate quickly after a neutron fluence of just 1.5313×10^{13} neutrons per square centimeter, which is even worse [82]. It was also observed that the tendency of this compound to absorb electromagnetic waves and convert them to heat decreases with increased neutron fluence [83].

Based on the small amount of data gathered about hexagonal boron nitride as far as neutron radiation is concerned, the compound appears to be a poor choice. However, the data really is inconclusive, and additional testing should be done before hexagonal boron nitride is discarded altogether as a possible vacuum vessel material.

4.6.0.3 Cubic Boron Nitride Cubic boron nitride is less characterized than hexagonal boron nitride, but the data that is available is fairly promising. At fluences of 8×10^{19} and 4×10^{20} neutrons per square centimeter, the compound

has shown decreases in density of 9 and 34 percent [84]. While a density decrease of 34 percent is likely far too large for the purposes of the vacuum vessel, considering that this effect will likely not be uniform and thus cause stress concentrations as well, a density decrease of 9 percent would be more acceptable, if not favorable.

From this information, cubic boron nitride could work well as far as neutron radiation goes for a space application, but would not work so well in a terrestrial setting. However, as mentioned with the other compounds, further testing should be undergone before making permanent decisions on the subject.

4.6.0.4 Boron Carbide Boron carbide, like boron nitride, is characterized well in the field of fission reactor design. However, much of the data available for it is in the form of captures per unit volume ρ_{cap}, which is different from neutron fluence. However, using the dimensions for boron carbide discussed previously in this study, and assuming total capture of the neutrons by the vacuum vessel, this can be calculated as shown in Equation 17 and Equation 18. This may be a rough estimate, but it is sure to be conservative, since it considers the maximum possible neutrons to be absorbed.

$$\rho_{cap,DFD} = \frac{6.11413 \times 10^{16}}{\pi \left((r_i + 31.5)^2 - r_i^2 \right) L} \cdot 3.15 \times 10^7 \cdot 4 = 1.52 \times 10^{18} \tag{17}$$

$$\rho_{cap,terr} = \frac{6.11413 \times 10^{16}}{\pi \left((r_i + 40.8)^2 - r_i^2 \right) L} \cdot 3.15 \times 10^7 \cdot 30 = 8.05 \times 10^{18} \tag{18}$$

In one study, 15 percent volume expansion occurred at a capture density of 10^{22} neutrons per cubic centimeter [85]. If this data is to be trusted, boron carbide is a fine choice for either application, for the fluence is much less than it would need to be to cause excessive swelling. This specific instance results in a burnup of boron-10 within the material of a little over 40 percent. Another source suggests that such a high burnup could result in minor cracking [86]. However, lower burnups, such as 20 percent, cause no detectable damage to the material, while still maintaining a high capture density limit of 0.5×10^{22} neutrons per cubic centimeter, which is still far in excess of what the vacuum vessel will require [85] [86].

Of all the materials presented so far, boron carbide is the most likely to function well under neutron radiation. However, it would still be best to test it in conditions more similar to those it will experience if it is chosen as the material for the vacuum vessel.

4.6.0.5 Lithium Hydride The resistance of lithium hydride to being damaged by neutron radiation is not well characterized. However, one cylindrical specimen tested under a fluence of 1.6×10^{17} neutrons per square centimeter over the course of about two days, and shows between 1 and 3 percent volume increase, which is minimal [87]. However, the appearance of swelling at such a low order of magnitude suggests that lithium hydride would struggle greatly with neutron fluences on the level the vacuum vessel will experience. Another study surmises through the analysis of lithium fluoride, which should be similar to lithium hydride, that lithium hydride is likely to form many voids and trap a significant amount of helium, possibly causing swelling of up to 80% by volume in the material [88].

The available data, sparse as it is, points to the failure of lithium hydride to suitably sustain the neutron loading expected. However, as with every compound, the reaction of lithium hydride to neutron fluence in the form it is to encounter as a part of the vacuum vessel ought to be tested further before the compound is discarded entirely.

Ultimately, it would seem that as far as neutron radiation is concerned, boron carbide is currently the most promising by far. However, not much is known, and further testing is required on all the compounds considered above. One thing that should be noted about the data gathered is that it contains next to no information about any properties other than swelling and mechanical strength when it comes to neutron radiation resistance. Properties such as thermal and electrical conductivity, specific heat, and reflectivity are important to compare before and after neutron radiation, and thus further testing is also needed on each of these compounds to discover how exactly their many properties change with prolonged neutron radiation exposure.

5 Properties Requiring Further Testing

During the course of this study, there were a number of properties that appeared not to have been tested for yet, or at least not by an organization who made the data accessible to the general public. One of the properties that was not

available was the reflectivity of each compound in the ranges that are significant to Bremsstrahlung and synchrotron radiation. Though some information could be found on thermal cycling, conclusive data on whether each material could withstand thermal cycling structurally as well as what its effect on the electrical, optical, and thermal properties of said materials would be was not available. Similarly, the effects of neutron radiation on each material was available in some specific situations, but very little data was available for the situation each material will have to tolerate when making up the vacuum vessel, not to mention the effects of said radiation on the other properties of the materials.

As a result of these knowledge gaps, it is clear that additional testing will be needed before any conclusive decisions on the vacuum vessel material are made. To start, numerous suppliers have been contacted to gather a list of purchasing options for test specimens of each of the boron compounds considered. Ultimately, the costs of appropriately-sized sputtering targets or sheets are in the range of $600 to $1000, and the cost of powders varies greatly based on the quantity in which they are ordered. The compiled list of suppliers and prices is included in **Appendix A**. Lithium hydride does not appear to be readily available in a bulk form, so it will need to be ordered from a company that can hot press it into a solid for our needs.

In addition to these compounds and knowledge gaps, parts made out of mixed lithium hydride and either beta-rhombohedral boron or hexagonal boron nitride are a possibility, and little to nothing is known about such a mixture. As a result, all the properties gathered for all other compounds need to be tested for in these compounds as well.

Reflectivity tests in the synchrotron and Bremsstrahlung ranges will likely be executable at the PFRC lab. Tests on how the specimens respond to thermal cycling and neutron radiation, however, may take significantly more effort, since the specimens must not only be observed under multiple levels of exposure to thermal cycling and neutron radiation, but also because at each stage practically all relevant properties must be tested as well, which will require a large amount of diverse equipment. Such testing would be an excellent future project.

6 Thermal Analysis of Cooling Channels

6.1 Basic Parameters of the Model

In order to do thermal analysis on the vacuum vessel with cooling channels both within and without the vessel, it is important first to know the properties of each material involved, which have been gathered in Table 4 and Table 5. Next, it is important to determine where sources and sinks of heat will be located in the vessel. Wherever the channels enter and exit the vessel in a given configuration, gaseous helium will flow in and out of the vessel. In between entry and exit, this gas will absorb heat from the walls of the vessel and carry it out, to be converted to useful work by a Brayton cycle heat engine. Bremsstrahlung radiation will ideally be absorbed fully by the tungsten lining of the cooling channels, so that the 0.15 MW of power emitted in the form of Bremsstrahlung by the FRC core, as presented in a previous paper [2], can be modeled as a surface heat source coming from the walls of the channel. The synchrotron radiation, on the other hand, will not be absorbed in this way, but will pass through the vacuum vessel normally. Though it is hoped that the synchrotron radiation will be reflected back into the core to assist in heating, it will eventually leave and pass through the vessel. Now, depending on the conductivity of the material used to construct the vacuum vessel, the synchrotron radiation, with a frequency of $f = 1.68 \times 10^{11}$ Hz, will be fully dissipated in the vessel over a different length, or may not fully dissipate at all, but continue to radiate past the vessel. A primitive model, presented in a textbook on classical electrodynamics [89], can be used to determine how quickly the radiation will dissipate. This model takes the form of skin depth δ, or the distance over which the radiation amplitude will attenuate to 37 percent of its initial value. The model is given in Equation 19. Note that it has been converted from Gaussian units as it was originally presented, and has been adjusted to take the desired inputs. The permeability μ will be assumed to be the vacuum value of $\mu = \mu_0 = 4\pi \times 10^{-7}$.

$$\delta = \sqrt{\frac{1}{\pi\mu f\sigma}} \tag{19}$$

For the purposes of this study, the radiation will be considered fully dissipated after a distance of $d_{\text{tot}} = 5 \cdot \delta$. This leads to at most 0.6 percent of the radiation continuing past the vessel, and since it is moving out from the center of a cylinder, there will be additional absorption due to increasing surface area as the radiation continues to spread outward, resulting in even more attenuation. If this region is less than half the thickness of the vessel, then the synchrotron radiation will be considered a surface source of heat from the inner wall, and if it is larger than half the thickness, the entire vessel will be considered a volume source of heat. In either event, this source will produce

the $P_s = 0.19$ MW of power emitted as synchrotron radiation [2]. Originally, the region over which the radiation dissapates was going to be considered a volume source of heat regardless, but doing this caused quite a bit of artificial thermal stress where the region ended and the vacuum vessel continued.

Where the total dissipation depth d_{tot} is larger than the thickness of the vessel, Equation 20 will be used to determine the power P_d dissipated in the material, where t is the thickness of the vessel, and the entire vessel will be considered a volume source for this energy.

$$P_d = P_s \cdot e^{-t/\delta} \tag{20}$$

All of the information described above is listed in Table 6. In this study, it is assumed that none of the compounds are enriched. Note that the values are calculated for two different temperatures. For each Solidworks trial, the values at 800 K are used, in order to evaluate the best case scenario in terms of radiation absorption for that material, which happens to be the worst case scenario as far as thermal stresses go.

	B	B4C	hBN	cBN	LiH w/ 2cm hBN
t_{space}	32.75	31.5	45.75	37.00	26.5
$t_{terrestrial}$	42.70	40.80	49.70	49.60	34.80
300 K					
δ (cm)	41.93	0.01	12279.07	1227.91	69.05
d_{tot} (cm)	209.64	0.03	61395.35	6139.54	345.25
$P_{d,space}$ (kW)	103	190	0.707	5.64	60.6
$P_{d,terrestrial}$ (kW)	121	190	0.767	7.52	75.2
800 K					
δ (cm)	0.01	0.00	549.27	38.83	0.84
d_{tot} (cm)	0.06	0.01	2746.34	194.15	4.18
$P_{d,space}$ (kW)	190	190	15.2	117	190
$P_{d,terrestrial}$ (kW)	190	190	16.4	137	190

Table 6: Calculated values for Solidworks heating component geometry.

One additional parameter is the speed of the helium gas through the cooling channels. This will impact mass flow, and will ultimately impact thermal stresses and Brayton cycle efficiency. In short, faster flows should cause less thermal gradients, and slower flows should result in higher-efficiency work extraction, because the maximum temperature of the flow is inversely related to the speed of the gas, with slower gasses lingering longer and thus being raised to higher temperatures. In these studies, mass flows of 0.05, 0.1, and 1.0 kilograms per second will be considered in order to gain an understanding of the effects of different amounts of helium flowing through the channels at different speeds. Each scenario was tested for the space application, where the vacuum is on both on the inner and on the outer surface of the vessel and so has no impact. In a terrestrial scenario, there would be an inward pressure force due to the lack of vacuum outside the vessel, but this was tested and proved to be inconsequential in the face of the stresses caused by thermal gradients. The geometry for the models was simplified as much as possible for the analysis, in order to check the feasibility of each option rather than to do a final analysis on a specific design.

6.2 Determining the Channel Entrance Temperature and Pressure

The final parameter that must be determined is the pressure of the helium when it enters the channels. To do this, the Brayton cycle to be used must be considered. A Brayton cycle consists of four looping processes: heat rejection, compression, heat addition, and work extraction. For this ideal case, the compressor and turbine will be considered to be isentropic, with the turbine extracting electricity through shaft work. Additionally, the heat rejection phase will be considered to be isobaric and at standard pressure ($P_{rej} = 101.325$ kPa), so as to allow a decent pressure ratio. Previous work has assumed a radiated power of $\dot{Q}_{out} = 170$ kW in the heat rejection stage for a space application, and though this may not fit the current scenario perfectly, especially for terrestrial applications, it will be adopted for this

study [2]. The helium entering the compressor will be assumed to be at a low temperature of $T_{comp} = 100$ K, though this is probably quite optimistic. A maximum temperature of $T_{turb} = 800$ K will be set at the inlet of the turbine.

From a trusted thermodynamics textbook, the specific heats $c_p = 5.1926\frac{\text{kJ}}{\text{kg·K}}$ and $c_v = 3.1156\frac{\text{kJ}}{\text{kg·K}}$ and the specific heat ratio $k = 1.667$ have been gathered for helium [90]. Assuming an ideal gas with constant, room-temperature specific heats, isobaric heat transfer processes, and isentropic turbomachinery, simple thermodynamic calculations result in Equation 21 and Equation 22 for the pressure P_{en} and temperature T_{en} at the entrance of the channel. These are approximations just to set the values necessary in Solidworks. Some of these Brayton cycle parameters will not emerge from the results of the simulation. An equation for pressure ratio r_p, which will be used later, is also defined in Equation 23.

$$P_{en,max} = P_{rej}\left(\frac{T_{turb}}{\frac{\dot{Q}_{out}}{c_p\dot{m}} + T_{comp}}\right)^{\frac{k}{k-1}} \tag{21}$$

$$T_{en,max} = \frac{T_{comp}T_{turb}}{\frac{\dot{Q}_{out}}{c_p\dot{m}} + T_{comp}} \tag{22}$$

$$r_{p,max} = \left(\frac{T_{turb}}{\frac{\dot{Q}_{out}}{c_v\dot{m}} + T_{comp}}\right)^{\frac{k}{k-1}} \tag{23}$$

These equations have been used to find the maximum inlet conditions and pressure ratios for each of the mass flows being studied. These values are laid out in Table 7. The chosen inlet conditions and pressure ratios that will actually be used are also displayed there. For the 1 kg/s case, the chosen values were for a new maximum temperature of $T_{turb} = 500$ K. Some materials, namely both polymorphs of boron nitride, allow some synchrotron radiation to escape. In these situations, the heat rejected is considered to be the fraction of Bremsstrahlung and synchrotron radiation combined that was absorbed times the original rejected power of $\dot{Q}_{out} = 170$ kW. Previous work with Brayton cycle analysis suggested values that were quite a lot different from the ones presented here, but they involved temperatures currently in excess of these material's capabilities, so this source is not relied on for this particular study [91].

$\dot{m}$	$P_{en,max}$	$T_{en,max}$	$r_{p,max}$	$P_{en,use}$	$T_{en,use}$	$r_{p,use}$
β-Rhombohedral Boron, Boron Carbide, and Lithium Hydride						
0.05	117	106	1.2	117	106	1.2
0.1	485	187	4.8	485	187	4.8
1	9023	602	89	2788	377	27.5
Hexagonal Boron Nitride						
0.05	513	191	5.1	513	191	5.1
0.1	1697	309	16.7	1697	309	16.7
1	12663	690	125.0	3991	431	38.6
Cubic Boron Nitride						
0.05	196	130	1.9	196	130	1.9
0.1	761	224	7.5	761	224	7.5
1	10338	636	102.0	3194	398	31.5

Table 7: Maximum and chosen values for the channel inlet.

This is all the information needed in order to effectively run simulations in Solidworks.

6.3 Brayton Efficiency

In addition to simulation parameters, it would also be helpful to calculate maximum possible Brayton cycle efficiency η for each option. To do this, Equation 24 is used, which was calculated using the same assumptions as before [90].

$$\eta = 1 - \frac{\dot{Q}_{out}}{\dot{m} \cdot c_p \cdot (T_{max,actual} - T_{comp} \cdot r_p^{\frac{k-1}{k}})} \tag{24}$$

6.4 Simulation Results

Many different configurations were analyzed. For each simulation executed, the different heat transfer rates, the maximum temperatures T_f and T_s of the fluid and solid respectively, the maximum power such a configuration would provide through a Brayton cycle, and the factor of safety with regards to thermal and pressure stresses are recorded. All of the simulations assumed a space application, so that no inward pressure forces would act on the vessel externally. The effect of such a pressure force was investigated and found to be inconsequential. Pressure effects from the helium in the channels are considered, however, so these results ought to be valid for terrestrial applications in all but thickness.

For each material considered, and for each of the three mass flows listed above, these tests were carried out on a model with eight smooth, straight channels parallel to the central axis within the vacuum vessel. The model used for this is displayed in Figure 10.

Figure 10: Depiction of the model used for thermal analysis with internal channels.

The results of these tests are displayed in Table 8. It is clear from the data that elemental boron and hexagonal boron nitride are the only compounds that come close to being able to withstand the thermal stresses they would be subjected to. Note that most configurations at the same mass flow get about the same output power, except for the boron nitride options, which allow too much synchrotron radiation to escape to get comparable power output, though hopefully that released energy will be reclaimed through another mechanism. Also, it should be noted that if the vessel is not constructed of one solid piece, some materials that appear to function very poorly here may prove feasible.

	$\dot{m}$ ($\frac{kg}{s}$)	$\dot{Q}_c$ (kW)	$\dot{Q}_r$ (kW)	$\dot{Q}_e$	T_f (K)	T_s (K)	η	P_{tot} (kW)	F.S.	V (m/s)
Smooth, Internal Channels
	0.05	93.10	245.16	0.00	1052	1168	0.31	28.55	0.64	1.50E-03
B	0.10	151.27	188.71	0.00	876	1025	0.52	79.36	0.85	1.28E-03
	1.00	274.57	65.39	0.00	562	713	0.82	226.08	1.92	4.47E-03
	0.05	85.85	253.95	0.00	862	896	0.13	11.34	0.24	1.50E-03
B$_4$C	0.10	154.62	185.47	0.00	777	815	0.44	68.78	0.30	1.28E-03
	1.00	279.39	60.61	0.00	550	593	0.81	226.63	0.63	4.47E-03
	0.05	25.59	139.61	174.80	622	622	0.26	6.66	0.84	2.41E-04
hBN	0.10	55.19	109.98	174.80	594	594	0.44	24.44	0.90	2.35E-04
	1.00	97.98	67.22	174.80	506	507	0.79	77.10	1.15	1.40E-03
	0.05	50.93	216.15	73.00	704	704	0.24	12.19	0.18	6.49E-04
cBN	0.10	105.62	161.39	73.00	653	653	0.49	51.81	0.21	5.76E-04
	1.00	196.43	70.58	73.00	521	522	0.82	161.62	0.33	2.44E-03
LiH	0.05	113.71	226.28	0.00	1596	1809	0.56	63.69	0.00	1.50E-03
w/ 2cm	0.10	196.12	143.93	0.00	1192	1506	0.67	132.21	0.00	1.28E-03
hBN	1.00	282.06	57.94	0.00	614	1072	0.86	243.16	0.00	4.47E-03

Table 8: Thermodynamic analysis results for smooth, internal channels.

Again for every material considered, these tests were executed on a model with external channels of stainless steel, as shown in Figure 11.
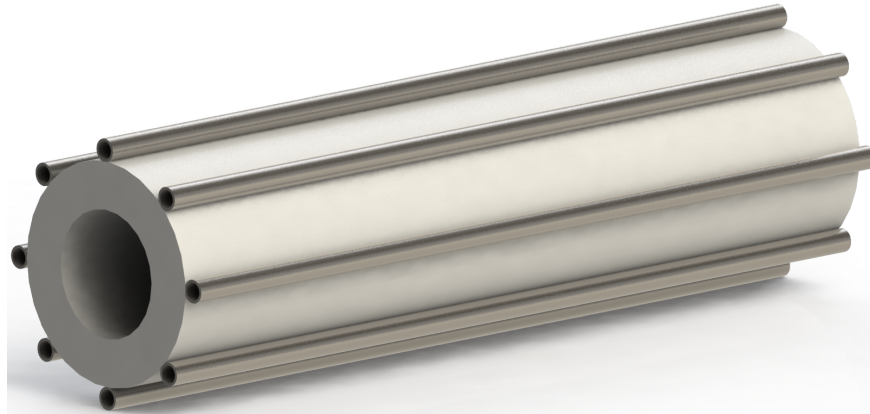
Figure 11: Depiction of the model used for thermal analysis with external channels.

This system was tested in the same way that the system with internal channels was, and the results of these simulations is included in Table 9. In the cases of elemental boron, boron carbide, and lithium hydride, internal channels are more effective at reducing thermal stresses and producing power output. However, hexagonal boron nitride is the opposite, benefiting greatly from external channels. This may be a result of its high thermal conductivity. Cubic boron nitride shows very little difference and no discernable trend between internal and external channels.

	$\dot{m}$ $(\frac{kg}{s})$	$\dot{Q}_c$ (kW)	$\dot{Q}_r$ (kW)	$\dot{Q}_e$	T_f (K)	T_s (K)	η	P_{tot} (kW)	F.S.	V (m/s)
Smooth, External Channels										
B	0.05	88.56	251.44	0.00	938	1047	0.21	18.73	0.68	1.50E-03
	0.10	140.00	200.00	0.00	739	1001	0.41	56.92	0.82	1.28E-03
	1.00	208.06	131.94	0.00	546	909	0.81	167.84	1.13	4.47E-03
B$_4$C	0.05	87.78	252.22	0.00	915	851	0.19	16.60	0.23	1.50E-03
	0.10	142.59	197.41	0.00	741	802	0.41	58.28	0.27	1.28E-03
	1.00	226.48	113.50	0.00	571	699	0.83	188.33	0.37	4.47E-03
hBN	0.05	44.08	126.96	174.80	1014	537	0.61	27.02	1.07	2.41E-04
	0.10	84.00	85.87	174.80	966	514	0.76	63.68	1.16	2.35E-04
	1.00	124.23	44.27	174.80	542	454	0.86	106.37	1.68	1.40E-03
cBN	0.05	58.90	208.07	73.00	883	684	0.42	24.74	0.19	6.49E-04
	0.10	113.67	153.33	73.00	729	636	0.57	64.48	0.23	5.76E-04
	1.00	179.07	87.89	73.00	542	554	0.85	151.95	0.31	2.44E-03
LiH w/ 2cm hBN	0.05	97.16	243.15	0.00	1051	1525	0.31	29.73	0.00	1.50E-03
	0.10	144.91	195.76	0.00	751	1483	0.42	60.75	0.00	1.28E-03
	1.00	197.35	144.86	0.00	576	1402	0.84	164.94	0.00	4.47E-03

Table 9: Thermodynamic analysis results for smooth, external channels.

Once these were tested, a couple of alternative methods were explored using β-rhombohedral boron and hexagonal boron nitride. The first of these was a set of axial channels as before, but this time with some ridges meant to encourage swirling introduced into the vessel. A view of this added feature is displayed in Figure 14.
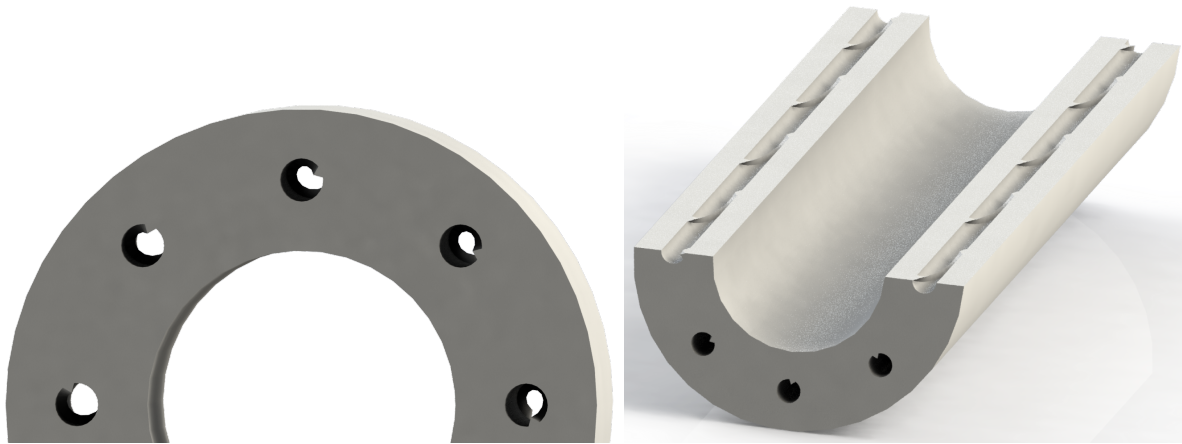
Figure 12: Depiction of the model used for thermal analysis with internally ridged channels.

The second and final alternative configuration analyzed was a model with channels that enter and exit the vessel radially, and which trace an azimuthal path around the vessel. This model was simulated with the same parameters as previously presented. The model used for this simulation is displayed in Figure 13.
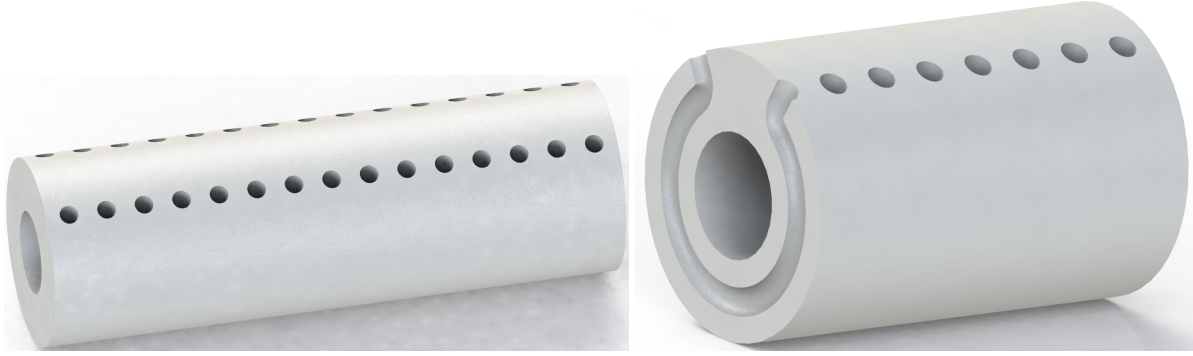
Figure 13: Depiction of the model used for thermal analysis with internal azimuthal channels.

The data for both of these alternative methods, using first hexagonal boron nitride and then β-rhombohedral boron, is included in Table 10. Perhaps unsurprisingly, ridged channels seem to help a great deal in regulating the temperature and keeping it low. They are also more efficient at lower mass flows than smooth channels, though they cease to be as efficient at higher mass flows. Rather than a flaw in the idea of ridged channels, it is likely that the pitch of the channels in the Solidworks model was simply better for lower flow speeds, and a higher pitch would allow improved efficiencies at higher speeds. Additionally unsurprisingly, the azimuthal channels turned out to be a complete disaster, generating much more severe thermal gradients and doing an attrocious job of regulating the temperatures in the vessel.

	$\dot{m}$ $(\frac{kg}{s})$	$\dot{Q}_c$ (kW)	$\dot{Q}_r$ (kW)	$\dot{Q}_e$	T_f (K)	T_s (K)	η	P_{tot} (kW)	F.S.	V (m/s)
				Internal channel alternatives made of hBN						
Ridged Channels	0.05	51.42	113.77	174.80	608	608	0.24	12.10	1.00	2.41E-04
	0.10	64.80	100.37	174.80	592	592	0.44	28.44	1.04	2.35E-04
	1.00	103.77	61.41	174.80	505	506	0.78	81.36	1.33	1.40E-03
Azimuthal Channels	0.05	33.23	131.98	174.80	635	635	0.28	9.37	0.73	2.41E-04
	0.10	32.40	132.80	174.80	637	637	0.52	16.71	0.74	2.35E-04
	1.00	95.55	69.63	174.80	522	522	0.82	78.78	0.98	1.40E-03
				Internal channel alternatives made of B						
Ridged Channels	0.05	116.88	223.05	0.00	1019	1133	0.28	32.91	0.69	1.50E-03
	0.10	164.96	175.02	0.00	885	1025	0.53	87.55	0.88	1.28E-03
	1.00	274.81	62.60	0.00	559	705	0.82	225.48	2.01	4.47E-03
Azimuthal Channels	0.05	59.27	280.73	174.80	1118	1214	0.66	38.91	0.42	1.50E-03
	0.10	115.76	224.20	174.80	1050	1147	0.79	90.93	0.56	1.28E-03
	1.00	255.59	84.40	174.80	643	823	0.92	236.38	1.26	4.47E-03

Table 10: Thermodynamic analysis results for alternative internal channel configurations using boron and hexagonal boron nitride.

Because of the success of the ridged channels in this simulation, both internal and external ridged channels were next simulated. The model used for the external ridged channels is shown in Figure 14.
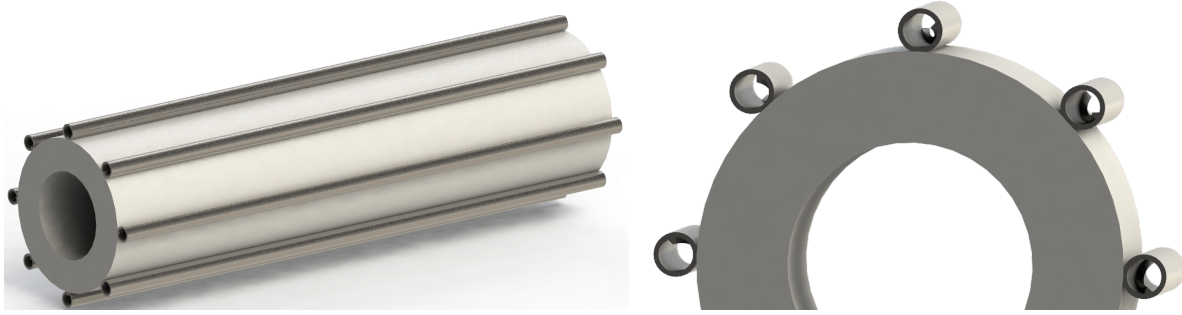
Figure 14: Depiction of the model used for thermal analysis with external ridged channels.

The simulation data gathered for internal and external channels with ridges is displayed in Table 11 and Table 12, respectively. The same trends can be seen as before when it comes to comparing internal and external channels. Additionally, however, the addition of ridges to the channels appears to almost universally lower stress in the vessel and raise the net power output in the process. There are a few exceptions at higher flow velocities, but these are likely due to the pitch of the ridges. Each test was performed with the same ridge pitch, but different pitches may optimal at different velocities. It is likely that the pitch chosen was simply more effective at lower velocities, and that a steeper pitch would work better at higher velocities.

	$\dot{m}$ ($\frac{kg}{s}$)	$\dot{Q}_c$ (kW)	$\dot{Q}_r$ (kW)	$\dot{Q}_e$	T_f (K)	T_s (K)	η	P_{tot} (kW)	F.S.	V (m/s)
				Ridged, Internal Channels						
B	0.05	116.88	223.05	0.00	1019	1133	0.28	32.91	0.69	1.50E-03
	0.10	164.96	175.02	0.00	885	1025	0.53	87.55	0.88	1.28E-03
	1.00	274.81	62.60	0.00	559	705	0.82	225.48	2.01	4.47E-03
B$_4$C	0.05	108.83	231.09	0.00	844	872	0.11	12.07	0.20	1.50E-03
	0.10	157.49	182.51	0.00	772	808	0.44	69.30	0.22	1.28E-03
	1.00	283.47	56.54	0.00	542	584	0.80	227.35	0.41	4.47E-03
hBN	0.05	51.42	113.77	174.80	608	608	0.24	12.10	1.00	2.41E-04
	0.10	64.80	100.37	174.80	592	592	0.44	28.44	1.04	2.35E-04
	1.00	103.77	61.41	174.80	505	506	0.78	81.36	1.33	1.40E-03
cBN	0.05	79.31	187.59	73.00	681	681	0.21	16.47	0.18	6.49E-04
	0.10	114.01	152.96	73.00	644	644	0.48	54.68	0.20	5.76E-04
	1.00	201.75	65.22	73.00	512	513	0.81	163.18	0.32	2.44E-03
LiH w/ 2cm hBN	0.05	142.09	197.93	0.00	1501	1753	0.53	75.32	0.00	1.50E-03
	0.10	195.54	144.46	0.00	1145	1492	0.66	128.69	0.00	1.28E-03
	1.00	270.44	58.39	0.00	636	1066	0.87	236.30	0.00	4.47E-03

Table 11: Thermodynamic analysis results for ridged, internal channels.

	$\dot{m}$ $(\frac{kg}{s})$	$\dot{Q}_c$ (kW)	$\dot{Q}_r$ (kW)	$\dot{Q}_e$	T_f (K)	T_s (K)	η	P_{tot} (kW)	F.S.	V (m/s)
				Ridged, External Channels						
B	0.05	113.44	226.57	0.00	959	999	0.23	26.20	0.76	1.50E-03
	0.10	142.09	197.97	0.00	747	972	0.42	58.97	0.87	1.28E-03
	1.00	189.98	150.03	0.00	531	914	0.79	149.69	1.12	4.47E-03
B_4C	0.05	112.06	228.23	0.00	961	813	0.23	26.08	0.24	1.50E-03
	0.10	144.13	195.93	0.00	752	784	0.42	60.57	0.27	1.28E-03
	1.00	209.14	131.31	0.00	580	715	0.84	175.47	0.36	4.47E-03
hBN	0.05	63.26	101.94	174.80	823	563	0.50	31.37	1.04	2.41E-04
	0.10	81.02	84.18	174.80	765	545	0.65	52.79	1.10	2.35E-04
	1.00	115.44	49.74	174.80	536	473	0.85	97.89	1.45	1.40E-03
cBN	0.05	84.15	182.89	73.00	840	671	0.38	32.39	0.20	6.49E-04
	0.10	117.90	149.13	73.00	749	640	0.58	68.82	0.23	5.76E-04
	1.00	187.14	79.86	73.00	539	546	0.85	158.20	0.32	2.44E-03
LiH w/ 2cm hBN	0.05	112.70	227.36	0.00	931	1524	0.20	23.08	0.00	1.50E-03
	0.10	154.94	185.18	0.00	775	1480	0.44	68.63	0.00	1.28E-03
	1.00	235.52	105.44	0.00	563	1349	0.82	194.15	0.00	4.47E-03

Table 12: Thermodynamic analysis results for ridged, external channels.

Ultimately, it would seem that producing a vacuum vessel with ridged channels out of hexagonal boron nitride is the best option in terms of temperatures and thermal gradients, while making one of β-rhombohedral boron is much better for the efficiency of the device. Additionally, higher mass flows appear to be both more efficient and better at regulating temperatures, contrary to the original expectation that higher mass flows would reduce efficiency. Therefore, it would be best if as high a mass flow of helium as possible was passed through the channels. It also appears that ridged channels have the potential to greatly increase the efficiency and thermal conditions in the vacuum vessel. As a result, both smooth and ridged channels must be examined in the case of hexagonal boron nitride, and the data for β-rhombohedral boron can be assumed to follow the same trends.

To investigate further the thermal conditions of hexagonal boron nitride, different channel diameters were examined to discover the best configuration of channels in the vacuum vessel. The results for internal and external channels are included in Table 13 and Table 14, respectively. It seems that generally the channel size has little impact on the device, but if one considers that larger channel sizes will be capable of sustaining higher mass flows, it is likely that larger channels would be more effective. Hexagonal boron nitride appears to function best when it has ridged, external channels, so such a configuration will be used to examine pitch. An internal channel configuration in elemental boron will also undergo these same examinations, to provide support for the universality of the trends investigated.

	$\dot{m}\,(\frac{kg}{s})$	$\dot{Q}_c$ (kW)	$\dot{Q}_r$ (kW)	$\dot{Q}_e$	T_f (K)	T_s (K)	η	P_{tot} (kW)	F.S.	V (m/s)
Internal Channels of hBN										
Smooth 10 cm	0.05	52.68	112.52	174.80	610	611	0.24	12.59	0.85	6.16E-04
	0.10	70.81	94.38	174.80	573	573	0.40	28.23	0.92	6.02E-04
	1.00	104.43	60.77	174.80	495	496	0.75	78.33	1.17	3.57E-03
Smooth 16 cm	0.05	25.59	139.61	174.80	622	622	0.26	6.66	0.84	2.41E-04
	0.10	55.19	109.98	174.80	594	594	0.44	24.44	0.90	2.35E-04
	1.00	97.98	67.22	174.80	506	507	0.79	77.10	1.15	1.40E-03
Ridged 10 cm	0.05	63.25	101.91	174.80	607	607	0.23	14.77	1.05	6.16E-04
	0.10	76.13	89.07	174.80	546	526	0.33	25.14	1.12	6.02E-04
	1.00	108.54	56.59	174.80	494	494	0.75	80.98	1.41	3.57E-03
Ridged 16 cm	0.05	51.42	113.77	174.80	608	608	0.24	12.10	1.00	2.41E-04
	0.10	64.80	100.37	174.80	592	592	0.44	28.44	1.04	2.35E-04
	1.00	103.77	61.41	174.80	505	506	0.78	81.36	1.33	1.40E-03

Table 13: Additional thermodynamic analysis results for internal channels in hexagonal boron nitride.

	$\dot{m}\,(\frac{kg}{s})$	$\dot{Q}_c$ (kW)	$\dot{Q}_r$ (kW)	$\dot{Q}_e$	T_f (K)	T_s (K)	η	P_{tot} (kW)	F.S.	V (m/s)
External Channels of hBN										
Smooth 10 cm	0.05	63.49	101.71	174.80	796	622	0.47	30.05	0.58	6.16E-04
	0.10	86.43	78.77	174.80	681	567	0.57	49.52	1.12	6.02E-04
	1.00	116.67	48.53	174.80	511	479	0.80	93.37	1.49	3.57E-03
Smooth 16 cm	0.05	44.12	126.96	174.80	1014	537	0.61	27.05	1.07	2.41E-04
	0.10	83.95	85.84	174.80	965	514	0.76	63.61	1.16	2.35E-04
	1.00	124.03	44.27	174.80	542	454	0.86	106.20	1.68	1.40E-03
Ridged 10 cm	0.05	76.58	88.62	174.80	816	587	0.49	37.54	1.08	6.16E-04
	0.10	92.67	72.54	174.80	710	547	0.60	55.96	1.19	6.02E-04
	1.00	119.73	45.48	174.80	518	467	0.82	97.75	1.56	3.57E-03
Ridged 16 cm	0.05	63.27	101.94	174.80	823	563	0.50	31.37	1.04	2.41E-04
	0.10	81.03	84.17	174.80	766	545	0.65	52.86	1.10	2.35E-04
	1.00	115.45	49.74	174.80	536	473	0.85	97.90	1.45	1.40E-03

Table 14: Additional thermodynamic analysis results for external channels in hexagonal boron nitride.

In general, it seems that ridged channels provide the highest performance, and that internal channels are better for most materials, with the exception of hexagonal boron nitride, which functions best with external channels. However, the pitch of the ridges should be altered to best match the decided mass flow. Since higher mass-flows are better, various mass flows of higher values should be tested in the future with various ridge pitches, to discover in general what the best pitch might be for a given mass flow for each configuration.

7 Material Comparison

Considering all previous properties and analyses, all the materials considered so far are compared in Table 15.

	β-B	hBN	cBN	B$_4$C	LiH
Mass	Good	Okay	Terrible	Good	Great
Cost	Terrible	Good	Okay	Good	Great
Conductivity	Bad	Great	Good	Terrible	Bad
Reflectivity	?	?	?	?	?
Thermal Cycling	Terrible	Great	Okay	Good	Bad
Neutron Radiation Resistance	?	Bad	Okay	Great	Bad
Mechanical Resilience under Operating Conditions	Good	Great	Bad	Bad	Bad

Table 15: High-level comparison of considered materials.

As is clear, there is no perfect option when it comes to a material for the vacuum vessel. However, hexagonal boron nitride and boron carbide have the most positive qualities, and if either of their reflectivities were to turn out to be poor, a thin film of a more favorable nature could be deposited on the inner wall of the vacuum vessel to ameliorate that problem. Lithium hydride is also a very attractive option only for mass and cost, and it is possible that a mix of it with hexagonal boron nitride would surpass all other materials.

8 Manufacturing

Once a material for the vacuum vessel is determined, the vacuum vessel must still be manufactured. Determining exactly how the vacuum vessel should be made and what manufacturing methods to use is a complicated and open-ended problem, and is discussed in detail here.

8.1 Design Considerations

The vacuum vessel itself is a long, cylindrical tube, about 5 meters in length, 70 centimeters in inner diameter, and 20 centimeters in thickness. One of its primary functions is shielding the superconducting coils and nearby operators from neutron radiation, and so it is important that the methods used to construct it maintain as high a density as possible in order to provide as much shielding as possible in the most mass-efficient way. The second function of the vacuum vessel is to maintain a vacuum, if possible, within the FRC chamber. This also requires that density be as high as possible, and that porosity be kept to a minimum in the manufacturing process. The final function of the vacuum vessel is to absorb heat from Bremsstrahlung radiation in channels lined with tungsten and extract it by running gaseous helium through the channels. These channels could be embedded in the vessel or be placed outside of it, and may end up being ridged or twisted, as discussed in a previous section. The channels will be be lined with tungsten somehow, perhaps as long strips or as a mesh. These channels may be complex features to manufacture, and this must be taken into account when choosing a manufacturing method. Additionally, whichever manufacturing method is chosen, it must be able to produce a vacuum vessel that has decent mechanical properties, so it will not be a likely point of failure for the device.

The vacuum vessel may be manufactured as one large tube, or it may be manufactured in any number of ways that allow smaller pieces to be manufactured first and then assembled somehow. In general, manufacturing many smaller sections would be much easier than manufacturing the entire vessel at once, and would allow the machines used to manufacture the vessel to remain a reasonable size. It would also makes future maintenance on the vacuum vessel easier, as damage or repairs to a single section would be possible, instead of a full replacement being required each time such maintenance is necessary. It would also allow design changes and upgrades to be implemented on individual sections, without the need to redesign the entire vacuum vessel. As a result, both will be considered when addressing the manufacturing methods that could be used.

8.2 Production of Boron Compounds

The materials considered for manufacturing the vacuum vessel in previous sections were β-rhombohedral boron, boron carbide, both structures of boron nitride, and lithium hydride. β-boron is only really produced in the form of powder through chemical vapor deposition or other precursor reduction processes, since it is not readily available in nature and is highly reactive in its amorphous form [92]. This is true of boron carbide [93] and hexagonal boron nitride [94] as well. Cubic boron nitride is generally manufactured by raising hexagonal boron nitride to extreme pressures [95], though it can also be created by other methods [96]. Either way, it too is only produced in powder form. Lithium hydride is also produced in powder form, though the process is much easier and cheaper than for boron compounds [97]. Though these compounds are often provided in the form of sputtering targets or thin films, these are still manufactured at the most basic level from their powder form [98]. As a result of the fundamental powder form of each of the compounds considered, the vacuum vessel will need to be manufactured using a process that involves the densification of this powder.

8.2.1 Traditional Powder Manufacturing Techniques

There are many traditional processes by which metal is manufactured from powder, and some of these can be used to produce ceramic materials out of powder as well. These methods are discussed here.

8.2.1.1 Cold Pressing (CP) The process of cold pressing simply involves pressing powder together at high pressures but standard temperatures. This does not work at all for boron compounds, and is not even considered for them. However, this method can create parts of lithium hydride at 95% theoretical density easily [97]. Because this is so easy, lithium hydride is not even considered with other traditional powder manufacturing methods.

8.2.1.2 Pressureless Sintering (PS) In pressureless sintering, powder of the manufacturing material is prepared and placed in a die in the shape of the part desired. Then, a punch is used to press the powder together tightly, producing a "green" part with very poor mechanical properties. Then, this part is heated to a high temperature below the melting temperature of the material, allowing the powder particles to fuse together into lower-energy arrangements, creating a solid part out of the "green" part [99].

This process has been used to produce boron carbide at up to 95 percent of its theoretical density, which is quite high for powder manufacturing, but does have some porosity [100]. This makes pressureless sintering a viable option for the vacuum vessel, if it is to be made of boron carbide. In addition, this method has been used on cubic boron nitride as well, with decent results [101], though in general cubic boron nitride is very difficult to control using sintering methods [102]. However, hexagonal boron nitride produces very porous parts when densified using this method [103], and this method cannot be used to produce parts out of elemental boron, if the part is to be crystalline and not amorphous [6].

It is important to note that with this process, it is quite difficult to make parts with complex geometries, since the entire part is to be compacted in a single direction. As a result, if the cooling channels are too complex, this method may work poorly, or else the channels will have to be machined in at a later time, and the tungsten added after the fact. This could potentially work for a material such as hexagonal boron nitride, which is easily machinable, but it would be exceedingly difficult if the vessel was made of a hard material such as boron carbide or cubic boron nitride. This will be true of any method that uses unidirectional pressing.

8.2.1.3 Hot Pressing (HP) Hot pressing involves placing powder in a mold or a die, as with pressureless sintering. However, unlike pressureless sintering, the powder is raised to very high temperatures as it is pressed by the punch to very high temperatures, effectively sintering the part as it is being pressed into the mold [104]. This process is more expensive than pressureless sintering, since the die has to withstand high temperatures as well as pressures, but the parts manufactured this way are much more dense than those manufactured by pressureless sintering, since the particles are pressed together while they are fusing.

Hot pressing has been used to produce boron carbide parts at 100 percent theoretical density [100], and parts produced using this method exhibited comparable thermal and mechanical properties to smaller specimens of boron carbide [105]. This makes it a highly desirable process for a vacuum vessel made of boron carbide, even more so than pressureless sintering. Elemental boron can also be pressed to 100 percent theoretical density this way, and regardless of the structure of the powder used, it results in a part of pure β-rhombohedral boron [6]. Hexagonal boron

nitride has been pressed to 97.6 percent theoretical density this way and exhibited favorable material properties as well [103]. Cubic boron nitride may be manufacturable this way, but it will likely have more complications than these other compounds [102].

As with pressureless sintering, if the channels in the vacuum vessel is too complex, than this method of manufacturing will have some significant challenges for materials that are difficult to machine, and even for those that aren't.

8.2.1.4 Hot Isostatic Pressing (HIP)   Hot isostatic pressing first involves pressing powder in a die, just as in pressureless sintering. Then, however, the "green" part is then placed in an environment of neutral gas and is then heated to high temperatures while being held at high pressures within the gas. This causes pressure to be exerted from all directions on the part, not just from one direction, as the particles fuse [105].

Hot isotactic pressing has been shown to produce even better properties in boron carbide than hot pressing alone [105]. This process could be used on all of the considered materials just as well as hot pressing can, but still has the drawback of unidirectional pressing when the powder is first being shaped into the "green" part.

Ultimately, these traditional techniques are all very similar, and few if any machines in existence are big enough to produce the vacuum vessel as a whole. However, if the pieces are made small enough, or machines are made much larger in the future, then the vessel should be manufacturable by these techniques.

8.2.2 Powder 3D-Printing Techniques

In recent years, 3D-printing has taken a larger and larger role in manufacturing. In 3D-printing, the part is constructed layer by layer. There are many modern 3D-printing techniques, some of which make direct use of powder to fabricate parts. However, regardless of the method, it should be noted that the vacuum vessel is very large compared to the standard print size of a 3D printer. As with traditional powder manufacturing, this will likely raise challenges in manufacturing the vacuum vessel, and larger printers or smaller sections will need to be developed or manufactured in order to make the vacuum vessel either way.

8.2.2.1 Selective Laser Melting (SLM)   In selective laser melting, a layer of powder is placed on the bed. Then, a laser selectively melts or sinters the area in the shape of the part, and then more powder is laid down and the process is repeated. This has the advantage of needing no support material, as the powder layers act as continuous support [106].

This method is very promising for powdered materials like the ones we have discussed so far, especially since it seemed from the traditional powder manufacturing techniques that the sintering and fusing of boron compounds in the form of powder was quite effective. Indeed, SLM printing has been implemented with boron carbide in the past. However, such attempts have been difficult, often leading to cracking or internal stresses in the parts, and even when successful, the material properties of the products left much to be desired. In one study, the boron carbide powder was coated in cobalt, producing a part with a porosity of 37 percent [107]. This is far too much porosity, and even if it wasn't, cobalt would increase the conductivity of the vacuum vessel, which is unacceptable, as it would cause too much energy in the rotating magnetic fields to be dissipated as resistive heat. When it comes to lithium hydride, the high coefficient of thermal expansion it has would make it even more difficult to work with. As a result, SLM may be a feasible option in the future, but currently the technology is not in a place where it can be readily applied to boron, boron carbide, or boron nitride powders.

8.2.2.2 Selective Laser Burnout (SLB)   This technique is relatively new, and has not been tested a lot yet. However, it has a lot of advantages and could be used once more developed, so it is considered here. In selective laser burnout, a slurry of the build powder as well as a binder that can be easily evaporated with increased temperature is made. Then, a layer of this slurry is laid down and dried. Next, a laser traces the outline of the part, evaporating the binder along the border. After that, another layer of the slurry is laid down, and the process is repeated. When the part is complete, it is removed from the rest of the dried slurry, since there is a layer of material with no binder in it traced three-dimensionally along its borders. This "green" part is removed and then pressurelessly sintered or hot isostatically pressed, evaporating the rest of the binder and creating a part made purely of the powder material [108]. Though this method of printing is not currently in use, it is in development and could become practical in the near future [109].

SLB printing has never been applied to boron, boron carbide, boron nitride, or lithium hydride. However, it has many promising characteristics that may make it, in the moderately near future, an effective process for manufacturing

the vacuum vessel of the PFRC. As a 3D printing method it could very easily produce a part with internal channels which would be too complex for a normal powder manufacturing process, and since it does not involve uniaxial pressing of the powder during the shaping of the "green" part, the complex channels would be just as strong as the rest of the vessel. Additionally, since SLB printing ultimately leaves behind no binder or filler material, it would allow all of the density of the vessel to be taken up by the compound used. Finally, as a printing process, it has higher speed than other methods due to only tracing the outline of the part, while having the sintering advantages of traditional powder manufacturing. In fact, the main disadvantage to hot isostatic pressing was that it still relied on uniaxial pressing of the initial powder part, an issue which SLB printing alleviates. Thus, it takes the flexibility and speed of the fastest 3D printing processes and adds it to the structural value of traditional hot isostatic pressing, making it a potentially excellent manufacturing method for the vacuum vessel.

Of these two options, both are not currently useful in manufacturing the vacuum vessel proposed. However, if technology were to advance significantly in this area in the coming years, SLB particularly would be a very attractive option, and may allow the manufacturing of a vacuum vessel with complex cooling channels.

8.3 Production of the Vacuum Vessel

In the production of the vacuum vessel itself, more must be considered than the method of manufacturing. It is also important to decide how to manufacture and assemble the vacuum vessel as a whole. Many options exist to do this, and a variety of options are presented in this section. It should be noted that for most of these options, either β-rhombohedral boron, boron nitride, or boron carbide could be used to construct the vessel. In these cases, hexagonal boron nitride is used, due to its overall superior properties and relative machinability, as discussed previously. However, in each case where boron nitride is used, it could be substituted for one of these other compounds without having an impact on the discussion. In addition, unless otherwise specified, the boron nitride powder is assumed to be hot-pressed to form the components described.

8.3.1 Option 1: Solid Boron Cylinder

The first and most obvious approach would be to simply construct the vacuum vessel in one solid piece of boron nitride. This piece will still need to be held in place somehow, and in this study this is accomplished using short alumina pegs. The vacuum vessel is to have cooling channels somewhere, whether on its surface or within it. Both of these options are considered here. In the subsequent configurations presented, cooling channels will be displayed if they are feasible within the design, but these two options always remain, and are assumed.

Option 1a: With Channels If channels are to be internal to the vessel, then they will need to be included axially, as shown in Figure 15.
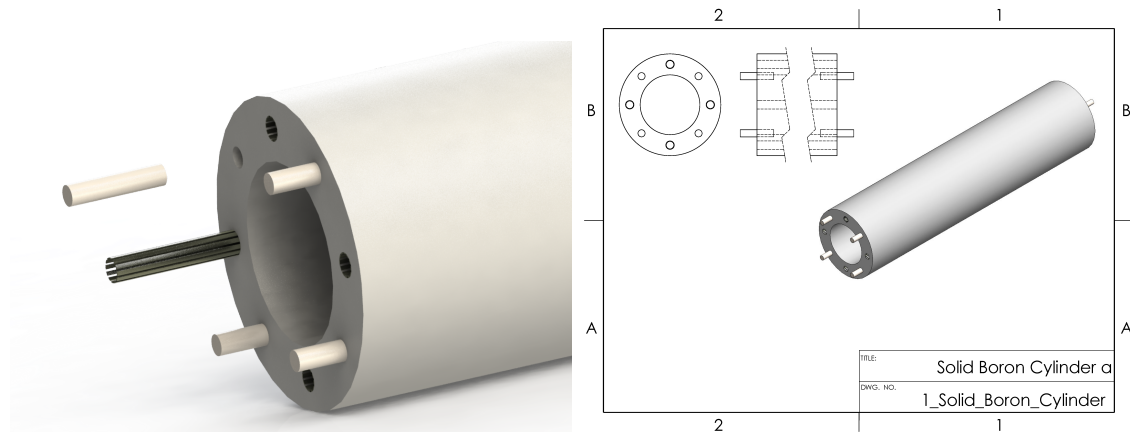
Figure 15: Visual description of **option 1a**.

Option 1b: Without Channels   If channels are to be external to the vessel, then they need not be considered in the construction of the vacuum vessel, a fact reflected in Figure 16.

Figure 16: Visual description of **option 1b**.

This option, in some ways, is the lightest option initially conceivable, at least constructed of boron nitride, since it requires no additional fasteners or anything to hold it together. It also can easily hold a vacuum without any additional measures, and is very simple to construct once manufactured. It provides seamless shielding of the neutrons as well. However, it provides no way to access the inside of the device to see what is occurring inside. Additionally, being one big piece, the thermal gradients that will inevitably span its length will stress the material significantly, though this stress will likely be much more intense if the cooling channels are included within the vessel as in **option 1a**, while thermal radiation will be greater if they are included without the vessel as in **option 1b**. Most importantly, this configuration is impossible to manufacture with the current technology available. There is not a hot press in the world that is big enough to manufacture it.

8.3.2   Option 2: Segmented Boron Cylinder

When considering manufacturing, it is always easier to make parts that are smaller than those that are larger. With this in mind, the vacuum vessel could be split into sections of solid boron nitride, and these sections could be lined up and pressed together on rails, as shown in Figure 17.
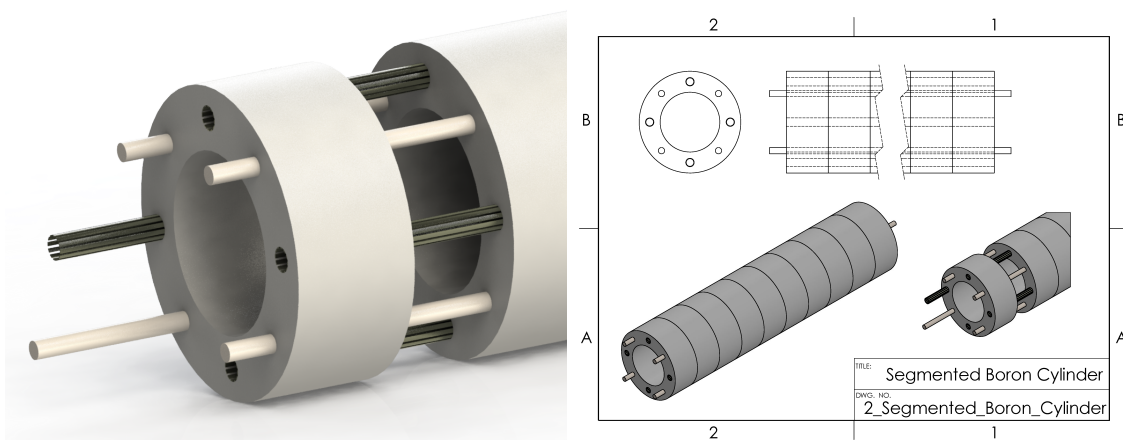
Figure 17: Visual description of **option 2**.

This option, being a variation of **option 1**, is still fairly light, though it may require slightly more weight in order to hold it together, and because the rails go all the way through it. However, unlike **option 1**, the inside of the device can be accessed fairly easily, and because it is constructed in segments, it should have increased tolerance to

thermal gradients compared to its predecessor. Unfortunately, the segmented quality of the vessel in this form makes it unable to hold a vacuum independently, and some neutrons are also likely to leak out along the planes where the segments meet. This configuration, like **option 1**, is still impossible to manufacture with current technology, though it is a much more reasonable size by comparison. Additionally, it comes with a bit more constructional complexity than **option 1**, though it is still fairly simple.

8.3.3   Option 3: Pie Slices

Going even further with the reasoning that led to **option 2**, individual sectors could be manufactured out of boron nitride and stacked side-by-side, while still being held in place by rails. This is depicted in Figure 18.
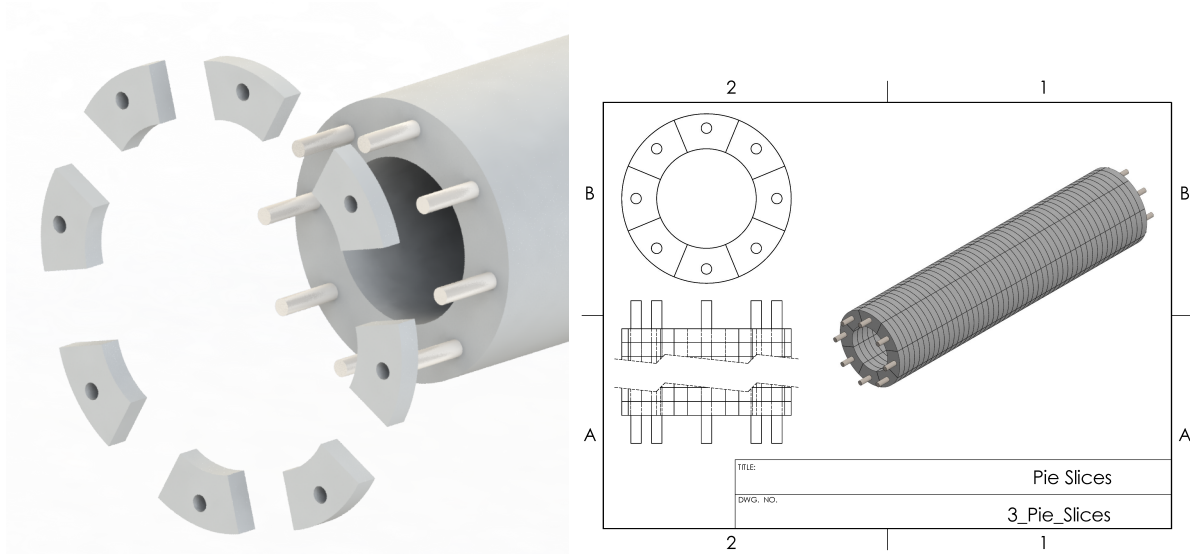
Figure 18: Visual description of **option 3**.

This option is likely to be a little heavier than **option 2**, since it is made of many more pieces that must be held together. Like **option 2**, it cannot hold a vacuum, and it has many more faces that neutrons would be able to escape through. On top of that, it is even more complex than the last option. However, this configuration is easily manufacturable by modern technology, and allows much more access to the FRC within than the other options so far. Finally, because of how small the pieces are, it should be much more tolerant of thermal gradients than **option 2**.

8.3.4   Option 4: Powder Packing

Another option could be the manufacturing and assembly of a thinner vessel by using smaller slices than in **option 3**, and then a thicker layer made of packaged powder of pure boron could be slid along the outside, as shown in Figure 19. This would allow the manufacturing of even smaller pieces of boron nitride.
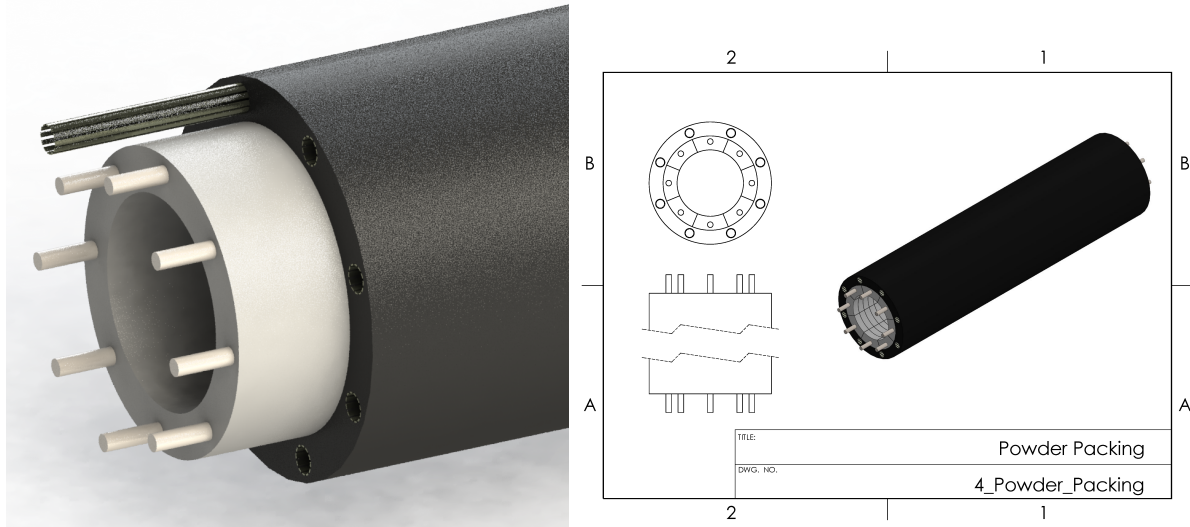
Figure 19: Visual description of **option 4**.

This option shares some things in common with **option 3**, including ease of manufacture at the cost of high complexity of construction. However, the powder layer offers seamless neutron shielding, stopping neutrons that escape from the faces where the slices of boron nitride meet. As before, it can handle thermal gradients with ease, and might even be able to hold a vacuum, depending on what is used to package the boron powder. Packaging the boron powder also adds weight to the design, however. Finally, due to the powder layer, access to the machine is essentially cut off, which would make instrumentation difficult.

8.3.5 Option 5: Layered Pie Slices

In order to reduce the possibility of neutrons passing through the surfaces of contact between sectors in **option 3**, two layers of such sectors could be manufactured. These layers could be designed in a staggered fashion, so that neutrons could only fully escape along single lines where the contact faces intersect, instead of through entire contact planes.

As was mentioned in the discussion of **option 3**, vacuum cannot be maintained with this method alone. Thus, an option is considered below to ameliorate this problem.

Option 5a: Free Slices   One option is to avoid attempting to make the configuration vacuum-tight, and instead simply allowing vacuum to be maintained from outside the bulk of the PFRC-4. This is depicted in Figure 20.
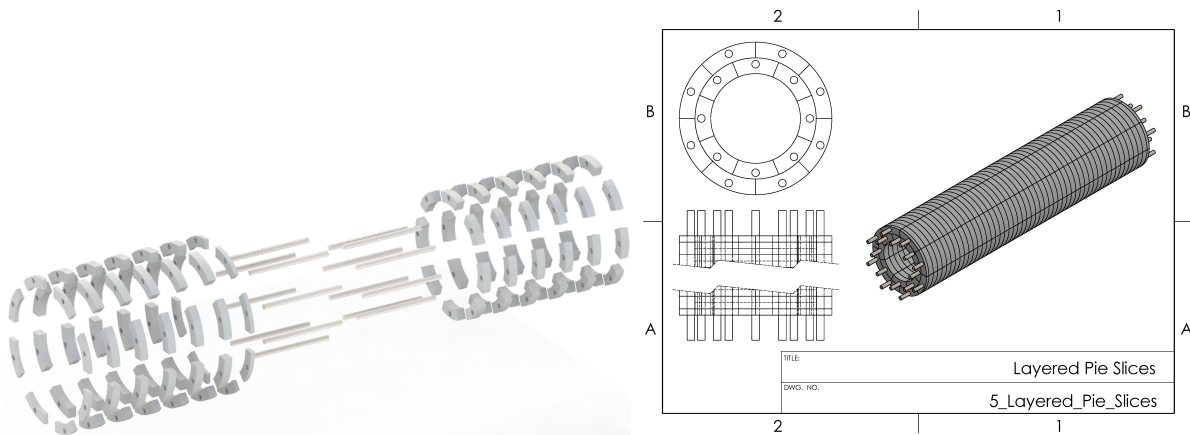
Figure 20: Visual description of **option 5a**.

34

Option 5b: Outer Reinforcement   Another choice is to place a layer of some strong, composite material outside of the configuration of **option 5a**, so that vacuum is maintained within the region of the slices in addition to the region containing the plasma. This is illustrated in Figure 21.
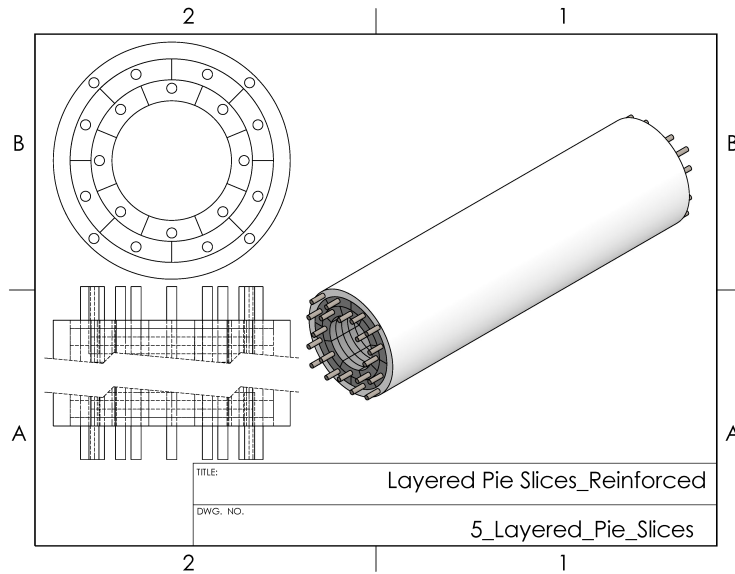
Figure 21: Visual description of **option 5b**.

This option bears much resemblance to **option 3**. It is made of small sections, which makes manufacturing easy, and is very high complexity. It can handle thermal gradients easily, but has a decent amount of extra weight necessitated by the rails which hold the sections in place. However, it also manages to shield more neutrons, as the only paths neutrons can take to avoid the assembly are single lines which, when the pieces are pressed together, will be very thin. **Option 5a** itself does not hold a vacuum, but it provides decent access to the device, and is not burdened by the slight extra weight of the composite shell. **Option 5b**, on the other hand, does have that extra weight, and can hold a vacuum as a result. The composite shell of **option 5b** also causes inhibited access to the inside of the device during operation.

8.3.6   Option 6: Segmented Boron Cylinder: 3D-Printed

Though the manufacturing method in each previous configuration was assumed to be hot-pressing, 3D-printing of boron nitride may be an option in the near future, as was discussed in the previous section. Specifically, the SLB method could provide a great way for producing dense structures made of boron nitride.

With this in mind, it may be possible to produce sections as described in the discussion of **option 2**, but with much more complex cooling channel geometry. One such possibility is displayed in Figure 22.
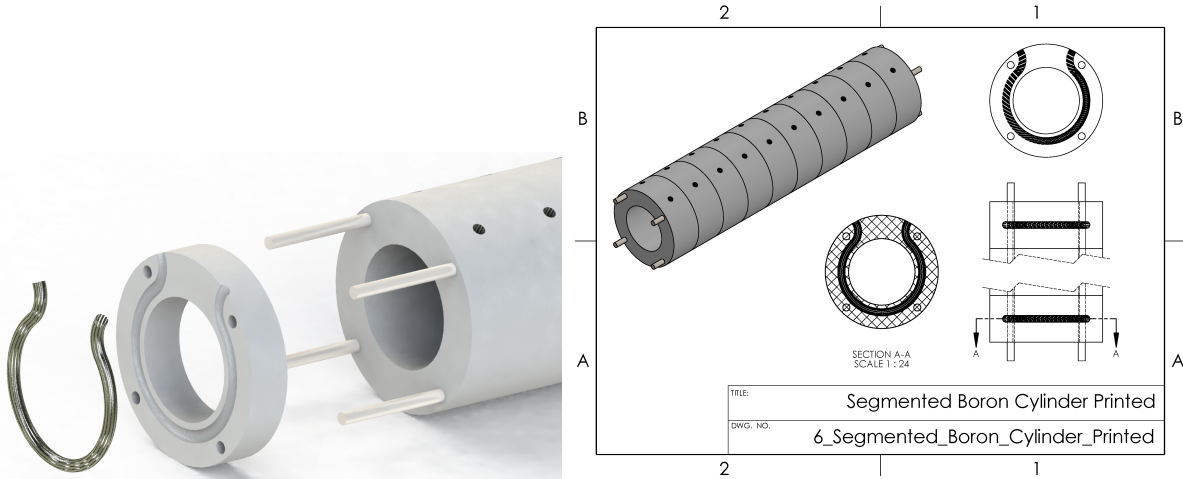
Figure 22: Visual description of **option 6**.

This configuration shares a lot in common with **option 2**, and while being unable to hold a vacuum, provides easy access to the device and allows neutrons out through the contact planes, as described earlier. The thermal gradients incurred by the cooling channel geometry specifically presented could be severe, but would need to be investigated further. The construction is no more complex than **option 2**, and for similar reasons, is still impossible to manufacture.

8.3.7 Option 7: Reinforced Powder Packing

In considering the manufacturing difficulties associated with producing any solid part out of boron nitride, another option, free of these difficulties, presents itself. One could simply manufacture a composite reinforcement layer to maintain vacuum and structural integrity from within. Then, a thick shell of boron powder could be packaged and slid around this internal reinforcement, as described in **option 4**. Such a vacuum vessel is described visually in Figure 23.

Figure 23: Visual description of **option 7**.

Relying on pure powder with a composite reinforcement has quite a few benefits. Though it may be a little heavier than other options owing to the low density of packed powder and the extra weight incurred by the packaging, it can hold a vacuum and has very low complexity. It can be manufactured with unprecedented ease, and can handle thermal gradients without any problems. Additionally, this option provides the seamless shielding described in **option 4** as well. However, the composite could be susceptible to neutron damage and thus failure, and leaves no avenue for accessing the device during operation.

8.3.8 Option 8: Borosilicate Glass

Up until this point, only boron nitride and other boron compounds have been considered in the configurations presented. However, other materials may also be feasible. One such material is borosilicate glass. If such a material worked, it could easily be cast as one solid piece, instead of being produced in sections. This is represented in Figure 24.
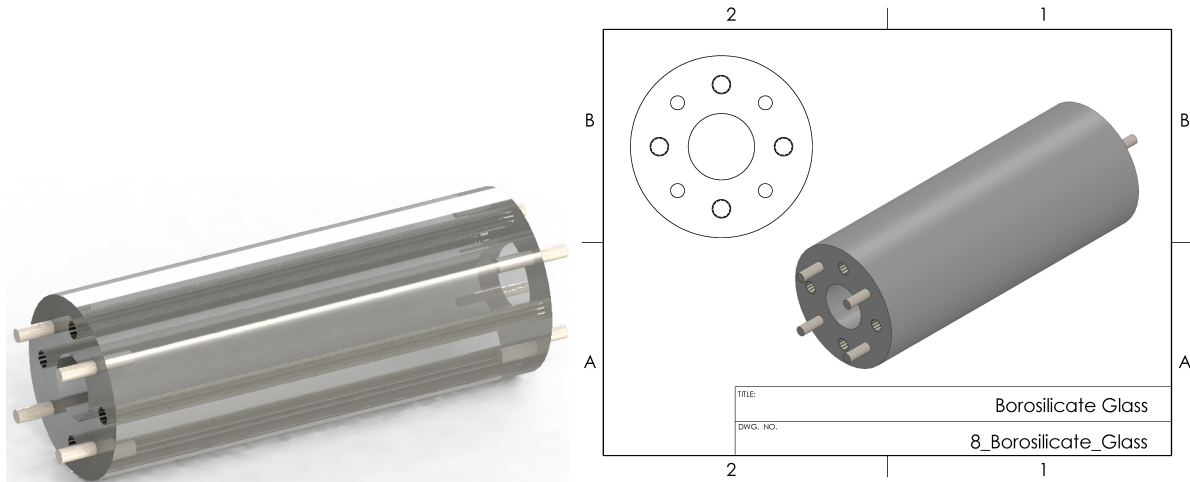
Figure 24: Visual description of **option 8**.

This option, first of all, is heavier than any other option presented in this study, as well as much thicker. This is a result of how sparse boron is in even the most boron-dense glasses. In addition, this option does not allow any access to the device within, and cannot handle high temperatures, which could be a significant issue. However, this configuration does hold a vacuum, and is very easy to manufacture. Once made, it would be very simple to assemble.

8.3.9 Option 9: Borosilicate Glass in 2 Layers

Considering the difficulty borosilicate glass poses due to its inability to withstand high temperatures, it is possible that incorporating a cooling layer, instead of just channels, between two cast cylindrical shells of borosilicate glass could keep the temperature below the failure temperature. This option is displayed in Figure 25.
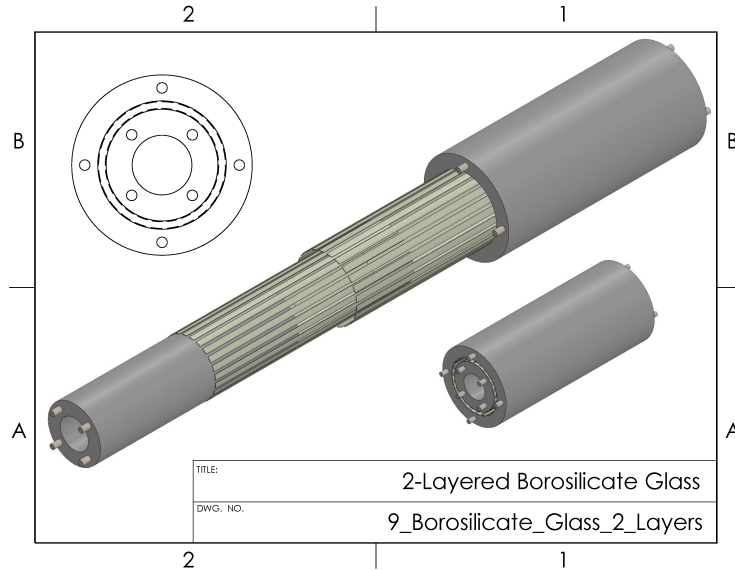
Figure 25: Visual description of **option 9**.

Being similar to **option 8**, this vacuum vessel design is also exceedingly heavy and thick, and makes it difficult to access the enclosed FRC. It still holds a vacuum and is easy to manufacture as well. The one difference here is that the cooling layer has the potential to lower the maximum temperature in the device, which would be of great benefit to borosilicate glass, and could actually make it viable if it worked. However, this does lead to slightly more constructional complexity.

8.3.10   Option 10: Scattering Approach

Laying borosilicate glass aside, another material option also exists. Lithium hydride, considered earlier throughout this study, could be used to scatter and thermalize neutrons, and then those neutrons could be absorbed by a thin layer of boron nitride, perhaps only a couple centimeters thick, as shown in Figure 26. Note that the dark outer layer represents boron nitride, which is naturally white, but is dark in the image to contrast with the lightly-colored lithium hydride.

Note that methods for manufacturing the lithium hydride pieces or assembling them could use any of the aforementioned methods that dealt with boron nitride, namely **options 1-7**.
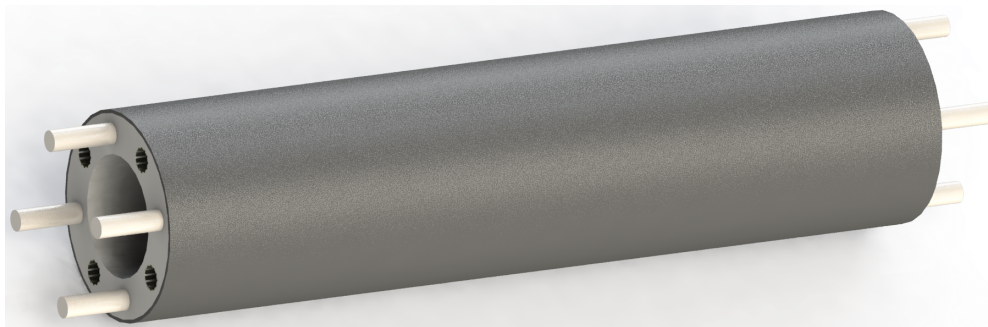
Figure 26: Visual description of **option 10**.

This option results in an incredibly light vessel, regardless of the details of its construction. However, it is not clear whether lithium hydride is capable of holding a vacuum, though it very well may be able to. Even more than that though, the conductivity of lithium hydride is high enough to be problematic to the FRC coils, which is an issue that must be resolved if this is to be a viable option.

8.3.11   Option 11: Reinforced Scattering Approach

In response to the possible inability of lithium hydride to hold a vacuum, it would be possible to add a polymer reinforcement to hold the vacuum at the innermost layer, similar to the one described in **option 7**. This option is depicted in Figure 27. Once more, this could be achieved by any number of construction methods, including those described by **options 1-7**.
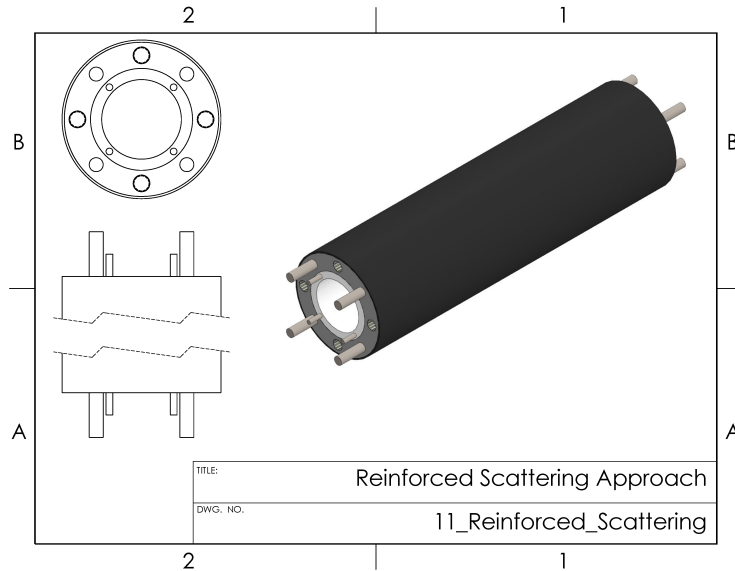
Figure 27: Visual description of **option 11**.

This is an identical design to **option 10**, except that it is very likely to hold a vacuum. It is still incredibly light as well. However, the conductivity of lithium hydride still poses a problem in this configuration. Additionally, if the composite used to reinforce this vessel within is sensitive to neutron damage, it could fail prematurely, and so the material for the internal reinforcement must be chosen with care.

8.3.12   Option 12: Reinforced Scattering Approach

A final option that could prove very effective would be to mix lithium hydride powder with boron or hexagonal boron nitride powder, and then use this mixture to manufacture the vacuum vessel. This mixture could still be used to construct the vacuum vessel by substituting it for boron nitride in **options 1-7**.
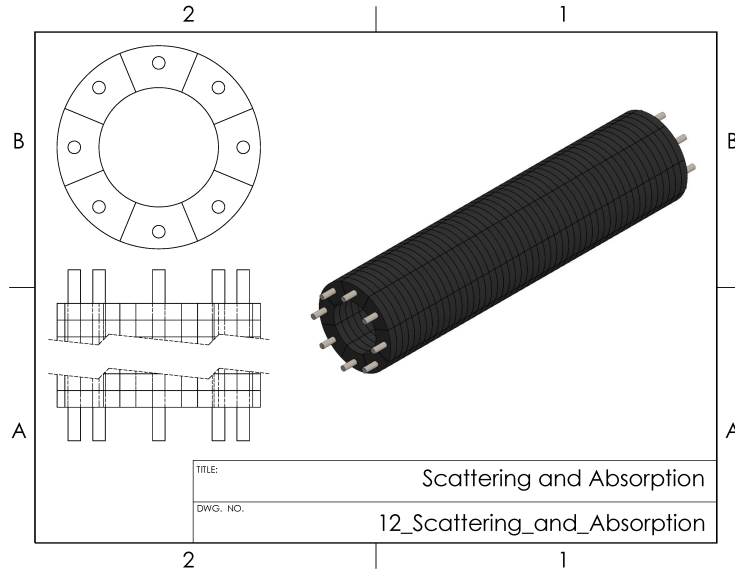
Figure 28: Visual description of **option 12**.

This option is meant to ameliorate the conductivity issue found in **options 10** and **11**, by separating the lithium hydride with boron or hexagonal boron nitride particles. The resulting vessel is heavier than the previous two options, but is still incredibly light in comparison to others, as was discussed in a previous section. This approach has the potential to be very effective, but it is not clear whether this new, mixed material will perform as desired. Very little is known about the mixture, and the emissivity, conductivity, strength, and tolerance to thermal gradients and neutron damage must be determined before it can be properly evaluated, which was also discussed previously.

8.4 Evaluation of Designs

A summary of all of the designs mentioned has been compiled and is available in Table 16. Spaceworthiness, or the suitability of the design for a DFD engine, is determined largely on the basis of weight. Terrestrial fitness, or the suitability of the design for a terrestrial power plant, is determined on both the ability of each design to hold a vacuum and the ease of access to the inside of the device that each design provides.

	1a	1b	2	3	4	5a	5b	6	7	8	9	10	11	12
Electrical	A	A	A	A	B	A	A	A	B	A	A	C	C	?
Weight	B+	B	B-	B-	C	B-	B-	B	C	F	F	A+	A+	A
Vacuum	A	A	F	F	?	F	A	F	A-	A	A	?	A	Depends,
Complexity	A	A	B-	C	C	D	D	B	A-	A	A-		Depends	and
Access	F	F	B	A	F	B	D	B	F	F	F		F	not much
Manufacturing	D-	D-	D	A	A	A	A	F	A	A	A	Depends		known
Shielding	A	A	B	C	A-	A-	A-	B	B+	A	A		Depends	about the
Thermal	F	C	B	A	A	A	A	B	A	D	D+			material.
Spaceworthiness	B	B	B	C	C	A-	B+	C	D	F	F	A+	A+	A
Terrestrial Fitness	B	B	B	B-	C	C	A	B	B	D	D	?	B	?

Table 16: A summary of the suitability of the proposed vacuum vessel designs.

From this information, it would seem that, for space applications, the best option would be to manufacture pieces from a powder mixture of lithium hydride and a boron compound, if the conductivity problem is indeed solved

by **option 12**, even though it is not the lightest option. However, if this does not solve the conductivity problem, simply tiling the boron nitride as in **option 5a** would likely function well.

For a terrestrial power plant, the best option by far is to tile boron nitride and reinforce it to hold a vacuum, as in **option 5b**. However, that composite reinforcement could actually be removed, and a vacuum could be imposed on the device from the outside. In this case, the container holding the vacuum could actually be constructed of stainless steel or something similar, and would not need to be included in the design of the tiled device at all, making perhaps **option 5a** best.

Ultimately, this list of designs is not exhaustive, and great thought must be put into exactly what method to use in manufacturing and constructing the vacuum vessel before making any final decisions.

9   Conclusion

Many considerations have been made for the construction of the PFRC-4 vacuum vessel. Elemental boron, boron carbide, boron nitride, and lithium hydride have been considered as materials for the vessel, along with brief looks at lithium deuteride, lithium tritide, and borosilicate glass. Nuclear, thermal, electrical, optical, and mechanical properties have been reported for each material, and a thermal and mechanical stress analysis was also carried out for each of these materials in a variety of cooling channel configurations. From this information, many insights were gleaned about which materials would be best for the construction of the vacuum vessel in different situations. Though no individual material proved to match all the criteria for the vessel, it is probable that hexagonal boron nitride or boron carbide, on account of their overall positive properties, or lithium hydride, on account of its low cost and mass, would be good options for the vacuum vessel.

Manufacturing options have also been considered at length, and it has been found that different methods are best suited for different applications. There are still many unknowns when it comes to finally choosing a material for the vacuum vessel and manufacturing it, and these must be investigated further through testing and simulations before making final decisions with regard to the vessel.

10   Acknowledgements

Appendix A: Testing Specimens and Powder Costs

In this appendix, prices are listed for sputtering targets and sheets of boron in Table 17 and Table 18 from different suppliers, as well as some powder costs for these compounds in Table 19. In the tables, materail (M), purity (P), grain size (G), percent theoretical density (Den), smoothness (S), crystal structure (C), and price, as well as dimensions such as diameter (D), thickness(T), width (W), and length (L), are listed in rows, as appropriate and as available. Crystal structures present include pyrolytic (pyr), hexagonal (hex), and rhombohedral (rhom), with pyrolytic being a specific type of hexagonal crystal structure.

Table 17: Sputtering target prices from various suppliers.

Vendor	M	P (%)	G (μm)	Den (%)	S (μm)	C	D (in)	T (in)	Price
Goodfellow	B	99.6					2.95	0.236	$1,126.00
Goodfellow	B	99.6					2.95	0.118	$1,775.00
Goodfellow	B	99.6					2	0.236	$1,300.00
Goodfellow	B	99.6					1.97	0.118	$1,300.00
Goodfellow	B4C						1.97	0.254	$975.00
Goodfellow	B4C						3	0.118	$610.00
Goodfellow	B4C						3	0.254	$1,150.00
Goodfellow	BN						2	0.118	$625.00
Goodfellow	BN						3	0.118	$675.00
Stanford Advanced Materials	B	99		55-60	3.2		2	0.125	$600.00
Stanford Advanced Materials	B	99		55-60	3.2		2	0.25	$630.00
Stanford Advanced Materials	B	99		55-60	3.2		3	0.125	$700.00
Stanford Advanced Materials	B	99		55-60	3.2		3	0.25	$730.00
Stanford Advanced Materials	B4C	99		85-90	3.2		2	0.125	$450.00
Stanford Advanced Materials	B4C	99		85-90	3.2		2	0.25	$480.00
Stanford Advanced Materials	B4C	99		85-90	3.2		3	0.125	$560.00
Stanford Advanced Materials	B4C	99		85-90	3.2		3	0.25	$600.00
Stanford Advanced Materials	BN	99		85-90	3.2	Hex	2	0.125	$450.00
Stanford Advanced Materials	BN	99		85-90	3.2	Hex	2	0.25	$480.00
Stanford Advanced Materials	BN	99		85-90	3.2	Hex	3	0.125	$560.00
Stanford Advanced Materials	BN	99		85-90	3.2	Hex	3	0.25	$600.00
Kurt J. Lesker Company	B	99.7		55			2	0.125	$839.00
Kurt J. Lesker Company	B	99.7		55			2	0.25	$874.00
Kurt J. Lesker Company	B	99.7		55			3	0.125	$1,030.00
Kurt J. Lesker Company	B	99.7		55			3	0.25	$1,119.00
Kurt J. Lesker Company	B4C	99.5		85	3.2		2	0.125	$621.00
Kurt J. Lesker Company	B4C	99.5		85	3.2		2	0.25	$679.50
Kurt J. Lesker Company	B4C	99.5		85	3.2		3	0.125	$748.00
Kurt J. Lesker Company	B4C	99.5		85	3.2		3	0.25	$814.50
Kurt J. Lesker Company	BN	99.5		90	3.2	Hex	2	0.125	$502.00
Kurt J. Lesker Company	BN	99.5		90	3.2	Hex	2	0.25	$616.00
Kurt J. Lesker Company	BN	99.5		90	3.2	Hex	3	0.125	$632.00
									Continued on next page

Vendor	M	P (%)	G (μm)	Den (%)	S (μm)	C	D (in)	T (in)	Price
Kurt J. Lesker Company	BN	99.5		90	3.2	Hex	3	0.25	$764.00
Himet Materials	B	99.9	40-70	50-55	3.2	Rhom	2	0.125	$399.00
Himet Materials	B	99.9	40-70	50-56	3.2	Rhom	3	0.125	$658.00
Himet Materials	B	99.9	40-70	50-57	3.2	Rhom	3	0.25	$814.00
Plasma Materials Inc.	B			55-60			2	0.125	$580.00
Plasma Materials Inc.	B			55-60			2	0.25	$690.00
Plasma Materials Inc.	B			55-60			3	0.125	$760.00
Plasma Materials Inc.	B			55-60			3	0.25	$880.00
Plasma Materials Inc.	B4C			55-60			2	0.125	$620.00
Plasma Materials Inc.	B4C			55-60			2	0.25	$740.00
Plasma Materials Inc.	B4C			55-60			3	0.125	$760.00
Plasma Materials Inc.	B4C			55-60			3	0.25	$890.00
Plasma Materials Inc.	BN			75		Hex	2	0.125	$480.00
Plasma Materials Inc.	BN			75		Hex	2	0.25	$620.00
Plasma Materials Inc.	BN			75		Hex	3	0.125	$630.00
Plasma Materials Inc.	BN			75		Hex	3	0.25	$760.00

Table 17: continued from previous page

Table 18: Sheet prices from Goodfellow.

Vendor	M	C	W x L (in x in)	T (in)	Price
Goodfellow	BN	Pyr	1.07 x 1.07	0.0394	$927.00
Goodfellow	BN		3.15 x 3.15	0.118	$820.00
Goodfellow	BN		1.07 x 1.07	0.157	$820.00
Goodfellow	B4C		1.969 x 1.969	0.0787	$695.00
Goodfellow	B4C		1.969 x 1.969	0.157	$1,163.00
Goodfellow	B4C		4 x 3.18	0.283	$1,298.00

Table 19: Powder prices from some suppliers.

Vendor	M	P (%)	G (μm)	C	Price	Amount (g)	Unit Price ($/g)
Goodfellow	B	98			$1,491.00	50	$29.82
Goodfellow	B4C	99			$824.00	500	$1.65
Goodfellow	BN	99.5		Hex	$901.00	500	$1.80
Advanced Abrasives	BN		0.2	Cub	$6,500.00	2000	$3.25
American Elements	LiH	99			$1,580.00	500	$3.16
American Elements	LiH	99			$1,083,720.00	2000	$0.54

References

[1] K. P. Griffin, M. T. Walsh, S. Cohen, R. Feder, J. Klabacha, and Q. Zhou, "Effects of neutron radiation and shielding recommendations for the pfrc-4," *PPST Undergraduate Internship Program Participants*, 2014.

[2] S. Thomas, M. Paluszek, S. Cohen, N. McGreivy, and E. Evans, "Fusion-enabled pluto orbiter and lander," 09 2017.

[3] K. Shirai, "Phase diagram of boron crystals," *Japanese Journal of Applied Physics*, vol. 56, p. 05FA06, apr 2017.

[4] V. L. Solozhenko, V. Z. Turkevich, and W. B. Holzapfel, "Refined phase diagram of boron nitride," *The Journal of Physical Chemistry B*, vol. 103, pp. 2903–2905, Apr 1999.

[5] H. Okamoto, "B-c (boron-carbon)," *Journal of Phase Equilibria*, vol. 13, aug 1992.

[6] C. Brodhag and F. Thevenot, "Hot pressing of various boron phases," *Journal of the Less Common Metals*, vol. 117, no. 1, pp. 175–180, 1986. Proceedings of the 8th international symposium on boron, borides, carbides, nitrides and related compounds.

[7] "Azo materials," June 2021. https://www.azom.com/properties.aspx?ArticleID=78.

[8] C. E. Messer, "A survey report on lithium hydride," 10 1960.

[9] J. D. Huba, *NRL PLASMA FORMULARY Supported by The Office of Naval Research*. Washington, DC: Naval Research Laboratory, 2013.

[10] P. K. Romano, N. E. Horelik, B. R. Herman, A. G. Nelson, B. Forget, and K. Smith, "Openmc: A state-of-the-art monte carlo code for research and development," *Annals of Nuclear Energy*, vol. 82, pp. 90–97, 2015. Joint International Conference on Supercomputing in Nuclear Applications and Monte Carlo 2013, SNA + MC 2013. Pluri- and Trans-disciplinarity, Towards New Modeling and Numerical Simulation Paradigms.

[11] N. Wilberg, *Inorganic Chemistry*. San Diego: Academic Press, 2001.

[12] "Goodfellow on-line interactive catalogue," June 2021. https://www.goodfellow.com/catalogue/GFCatalogue.php.

[13] "Millipore sigma," July 2021. https://www.sigmaaldrich.com/US/en/product/aldrich/601551?context=product.

[14] X. Zhang and J. Meng, "Chapter 4 - recent progress of boron nitrides," in *Ultra-Wide Bandgap Semiconductor Materials* (M. Liao, B. Shen, and Z. Wang, eds.), Materials Today, pp. 347–419, Elsevier, 2019.

[15] "cbpn cubic boron nitride powder," July 2021. https://advancedabrasives.com/index.cfm?page=sap-cbn-powder.

[16] H. Werheit and H. G. Leis, "On the conductivity mechanism of β-rhombohedral boron," *physica status solidi (b)*, vol. 41, no. 1, pp. 247–253, 1970.

[17] L. Vel, G. Demazeau, and J. Etourneau, "Cubic boron nitride: synthesis, physicochemical properties and applications," *Materials Science and Engineering: B*, vol. 10, no. 2, pp. 149–164, 1991.

[18] F. W. Glaser, D. Moskowitz, and B. Post, "An investigation of boron carbide," *Journal of Applied Physics*, vol. 24, no. 6, pp. 731–733, 1953.

[19] L. V. Astaf'eva, F. F. Gavrilov, B. L. Dvinyaninov, and V. P. Panov, "Electrical conductivity and photoconductivity of single crystals of lithium hydride," *Soviet Physics Journal*, vol. 14, pp. 1385–1388, Oct 1971.

[20] L. G. Carpenter and P. J. Kirby, "The electrical resistivity of boron nitride over the temperature range 700 degrees c to 1400 degrees c," *Journal of Physics D: Applied Physics*, vol. 15, pp. 1143–1151, jul 1982.

[21] C. Wood and D. Emin, "Conduction mechanism in boron carbide," *Phys. Rev. B*, vol. 29, pp. 4582–4587, Apr 1984.

[22] A. Pramanick, P. P. Dey, and P. K. Das, "Microstructure, phase and electrical conductivity analyses of spark plasma sintered boron carbide machined with wedm," *Ceramics International*, vol. 46, no. 3, pp. 2887–2894, 2020.

[23] E. Hecht, *Optics, Global Edition*. Essex, England: Pearson Education, Inc., 5th edition. ed., 2017.

[24] F. L. Gebhart and V. P. Jacobsmeyer, *The Optical and Electrical Constants of Beta-Rhombohedral Boron*, pp. 133–141. Boston, MA: Springer US, 1965.

[25] K. Sidorin, M. Karin, V. Bobrikov, A. Shelykh, G. Tsagareishvili, D. Gabun1ya, G. Tavadze, and M. Korsukova, "Optical properties of single-crystal β rhombohedral boron in the range of fundamental absorption," *Journal of the Less Common Metals*, vol. 82, pp. 297–302, 1981.

[26] N. Morita and A. Yamamoto, "Optical and electrical properties of boron," *Japanese Journal of Applied Physics*, vol. 14, pp. 825–832, jun 1975.

[27] H. Binnenbruck and H. Werheit, "Lattice vibrations and optical properties of β-rhombo-hedral boron in the far-ir region," *Journal of the Less Common Metals*, vol. 47, pp. 91–96, 1976.

[28] M. Fernández-Perea, J. I. Larruquert, J. A. Aznárez, J. A. Méndez, M. Vidal-Dasilva, E. Gullikson, A. Aquila, R. Soufli, and J. L. G. Fierro, "Optical constants of electron-beam evaporated boron films in the 6.8-900 ev photon energy range," *J. Opt. Soc. Am. A*, vol. 24, pp. 3800–3807, Dec 2007.

[29] E. Kierzek-Pecold, J. Kołodziejczak, and I. Pracka, "Optical constants of β-rhombohedral boron in the region 1.2 to 6.2 ev," *physica status solidi (b)*, vol. 22, no. 2, pp. K147–K150, 1967.

[30] H. Werheit, A. Hausen, and H. Binnenbruck, "Optical anisotropy of β-rhombohedral boron from 0.4 to 16 μm," *physica status solidi (b)*, vol. 51, no. 1, pp. 115–121, 1972.

[31] S. Adachi, *Hexagonal Boron Nitride (h-BN)*, pp. 127–136. Boston, MA: Springer US, 1999.

[32] A. Zunger, A. Katzir, and A. Halperin, "Optical properties of hexagonal boron nitride," *Phys. Rev. B*, vol. 13, pp. 5560–5573, Jun 1976.

[33] D. M. Hoffman, G. L. Doll, and P. C. Eklund, "Optical properties of pyrolytic boron nitride in the energy range 0.05—10 ev," *Phys. Rev. B*, vol. 30, pp. 6051–6056, Nov 1984.

[34] D. Jin-Xiang, Z. Xiao-Kang, Y. Qian, W. Xu-Yang, C. Guang-Hua, and H. De-Yan, "Optical properties of hexagonal boron nitride thin films deposited by radio frequency bias magnetron sputtering," *Chinese Physics B*, vol. 18, pp. 4013–4018, sep 2009.

[35] Y. Cai, L. Zhang, Q. Zeng, L. Cheng, and Y. Xu, "Infrared reflectance spectrum of bn calculated from first principles," *Solid State Communications*, vol. 141, no. 5, pp. 262–266, 2007.

[36] D. H. Berns and M. A. Cappelli, "Low energy ion impact-enhanced growth of cubic boron nitride in a supersonic nitrogen/argon plasma flow," *Journal of Materials Research*, vol. 12, pp. 2014–2026, Aug 1997.

[37] N. Miyata, K. Moriki, O. Mishima, M. Fujisawa, and T. Hattori, "Optical constants of cubic boron nitride," *Phys. Rev. B*, vol. 40, pp. 12028–12029, Dec 1989.

[38] P. J. Gielisse, S. S. Mitra, J. N. Plendl, R. D. Griffis, L. C. Mansur, R. Marshall, and E. A. Pascoe, "Lattice infrared spectra of boron nitride and boron monophosphide," *Phys. Rev.*, vol. 155, pp. 1039–1046, Mar 1967.

[39] M. I. Eremets, M. Gauthier, A. Polian, J. C. Chervin, J. M. Besson, G. A. Dubitskii, and Y. Y. Semenova, "Optical properties of cubic boron nitride," *Phys. Rev. B*, vol. 52, pp. 8854–8863, Sep 1995.

[40] R. Lalngaihawmi and R. Thapa, "Study of electronic and optical properties of boron nitride," *International Journal of Innovative Science, Engineering & Technology*, vol. 2, pp. 2348–7968, July 2015.

[41] S. Adachi, *Optical Constants of Crystalline and Amorphous Semiconductors*. Springer US, 1999.

[42] O. Kutsay, C. Yan, Y. Chong, Q. Ye, I. Bello, W. Zhang, J. Zapien, Z. Zhou, Y. Li, V. Garashchenko, A. Gontar, N. Novikov, and S. Lee, "Studying cubic boron nitride by raman and infrared spectroscopies," *Diamond and Related Materials*, vol. 19, no. 7, pp. 968–971, 2010. Proceedings of Diamond 2009, The 20th European Conference on Diamond, Diamond-Like Materials, Carbon Nanotubes and Nitrides, Part 2.

[43] J. L. Lauer, "Optical constants of boron carbide," tech. rep., Rensselaer Polytechnic Institute, 08 1981.

[44] R. Soufli, A. L. Aquila, F. Salmassi, M. Fernández-Perea, and E. M. Gullikson, "Optical constants of magnetron-sputtered boron carbide thin films from photoabsorption data in the range 30 to 770 ev," *Appl. Opt.*, vol. 47, pp. 4633–4639, Sep 2008.

[45] "Composition dependent microstructure and optical properties of boron carbide (bxc) thin films deposited by radio frequency-plasma enhanced chemical vapour deposition technique," *Materials Research Bulletin*, vol. 109, pp. 175–182, 2019.

[46] A. A. Ahmad, N. J. Ianno, P. G. Snyder, D. Welipitiya, D. Byun, and P. A. Dowben, "Optical properties of boron carbide (b5c) thin films fabricated by plasma-enhanced chemical-vapor deposition," *Journal of Applied Physics*, vol. 79, no. 11, pp. 8643–8647, 1996.

[47] H. Werheit, A. Leithe-Jasper, T. Tanaka, H. Rotter, and K. Schwetz, "Some properties of single-crystal boron carbide," *Journal of Solid State Chemistry*, vol. 177, no. 2, pp. 575–579, 2004. Boron, Borides and Related Compounds Proceedings of the 14th Inte rnaitonal Symposium on Boron, Borides and Related Compounds.

[48] H. Binnenbruck and H. Werheit, "Ir-active phonons of boron and boron carbide," *Zeitschrift Fur Naturforschung Section A-a Journal of Physical Sciences - Z NATURFORSCH SECT A*, vol. 34, 05 1979.

[49] H. Werheit and U. Kuhlmann, "Superconductivity in boron carbide? clarification by low-temperature MIR/FIR spectra," *Journal of Physics: Condensed Matter*, vol. 23, p. 435501, oct 2011.

[50] G. A. Samara, H. L. Tardy, E. L. Venturini, T. L. Aselage, and D. Emin, "Ac hopping conductivities, dielectric constants, and reflectivities of boron carbides," *Phys. Rev. B*, vol. 48, pp. 1468–1477, Jul 1993.

[51] U. Kuhlmann, H. Werheit, and K. Schwetz, "Distribution of carbon atoms on the boron carbide structure elements," *Journal of Alloys and Compounds*, vol. 189, no. 2, pp. 249–258, 1992.

[52] S. Banger, V. Nayak, and U. Verma, "Hydrogen storage in lithium hydride: A theoretical approach," *Journal of Physics and Chemistry of Solids*, vol. 115, pp. 6–17, 2018.

[53] T. Miki, M. Ikeya, Y. Kondo, and H. Kanzaki, "Reflectance spectrum of lithium hydride at the li k-absorption edge," *Solid State Communications*, vol. 39, no. 5, pp. 647–649, 1981.

[54] V. A. Pustovarov, "Reflection spectra of lithium hydride (deuteride) crystals in the 4–35 ev energy range," *Technical Physics Letters*, vol. 40, pp. 590–593, Jul 2014.

[55] "Matweb material property data," July 2021. http://www.matweb.com/index.aspx.

[56] J. Nash, "Reflector and shield material properties for project prometheus," 11 2005.

[57] P. R. H. Türkes, E. T. Swartz, and R. O. Pohl, "Thermal properties of boron and boron carbides," *AIP Conference Proceedings*, vol. 140, no. 1, pp. 346–361, 1986.

[58] "Technical products, inc.," June 2021. http://www.technicalproductsinc.com/.

[59] F. R. Corrigan, "Thermal conductivity of polycrystalline cubic boron nitride compacts," 1979.

[60] H. Nastelin, "Determination of the emissivity of materials. interim final report," *Technical Management: National Aeronautics and Space Administration, Lewis Research Center, Nuclear Technology Branch*, 1961-1963.

[61] T. Lundström, B. Lönnberg, and J. Bauer, "Thermal expansion of β-rhombohedral boron," *Journal of Alloys and Compounds*, vol. 267, no. 1, pp. 54–58, 1998.

[62] M. A. White, A. B. Cerqueira, C. A. Whitman, M. B. Johnson, and T. Ogitsu, "Determination of phase stability of elemental boron," *Angewandte Chemie International Edition*, vol. 54, no. 12, pp. 3626–3629, 2015.

[63] G. Pristáš, H. Werheit, S. Gabáni, S. Shalamberidze, and K. Flachbart, "Low temperature specific heat anomaly with boson peak in isotope-enriched boron carbides $b_{4.3}c - b_{10}c$," *Solid State Sciences*, vol. 101, p. 106140, 2020.

[64] V. L. Solozhenko, V. Z. Turkevich, and W. B. Holzapfel, "Refined phase diagram of boron nitride," *The Journal of Physical Chemistry B*, vol. 103, pp. 2903–2905, Apr 1999.

[65] A. Simpson and A. D. Stuckes, "The thermal conductivity of highly oriented pyrolytic boron nitride," *Journal of Physics C: Solid State Physics*, vol. 4, pp. 1710–1718, sep 1971.

[66] P. R. H. Türkes, E. T. Swartz, and R. O. Pohl, "Thermal properties of boron and boron carbides," *AIP Conference Proceedings*, vol. 140, no. 1, pp. 346–361, 1986.

[67] D. M. I. Center, *The Properties of Boron*. Columbus, Ohio: Battelle Memorial Institute, 1960.

[68] V. I. Matkovich, *Boron and Refractory Borides*. Springer-Verlag Berlin Heidelberg New York 1977, 1977.

[69] "Boron nitride," August 2021. https://precision-ceramics.com/materials/boron-nitride/.

[70] "Precision ceramic," June 2021. https://www.teatrobelarte.co/boron-nitride-ceramics-price-for-sale_23354/.

[71] D. Carolan, A. Ivanković, and N. Murphy, "Thermal shock resistance of polycrystalline cubic boron nitride," *Journal of the European Ceramic Society*, vol. 32, no. 10, pp. 2581–2586, 2012.

[72] L. Begrambekov, A. Grunin, N. Puntakov, Y. Sadovskiy, V. Budaev, and S. Grashin, "In situ renewable coating of boron carbide (b4c) for plasma materials for plasma-technological and fusion devices," in *Paint and Coatings Industry* (F. Yilmaz, ed.), ch. 7, Rijeka: IntechOpen, 2019.

[73] H. Greuner, M. Balden, B. Boeswirth, H. Bolt, R. Gadow, P. Grigull, G. Hofmann, T. Huber, W. Kasparek, H. Kumric, S. Lindig, G. Matern, M. Mayer, R. Neu, H. Renner, J. Roth, M. Riegert-Escribano, J. Simon-Weidner, and R. Wacker, "Evaluation of vacuum plasma-sprayed boron carbide protection for the stainless steel first wall of wendelstein 7-x," *Journal of Nuclear Materials*, vol. 329-333, pp. 849–854, 2004. Proceedings of the 11th International Conference on Fusion Reactor Materials (ICFRM-11).

[74] J. Coad, B. Farmery, J. Linke, and E. Wallura, "Experience with boron-carbide coated target tiles in jet," *Journal of Nuclear Materials*, vol. 200, no. 3, pp. 389–394, 1993.

[75] Y. Hishinuma, M. Akoshima, Y. Yamashita, T. Tanaka, A. Sagara, and T. Muroga, "Effect of heat cycling on microstructure and thermal property of boron carbide sintered bulk as a shielding material for fusion blanket," *Plasma and Fusion Research*, vol. 9, June 2014.

[76] L. Manning and D. J. McKee, "Investigation of the effective thermal conductivity of cast lithium hydride," 6 1961.

[77] F. B. Waldrop, "Lithium hydride as a mobile neutron shield," 2 1958.

[78] J. J. Swab, L. Vargas-Gonzalez, E. Wilson, and E. Warner, "Properties and performance of polycrystalline cubic boron nitride," *International Journal of Applied Ceramic Technology*, vol. 12, no. S3, pp. E74–E81, 2015.

[79] V. K. Golubev and K. G. Rabinovich, "Influence ff the initial state on the strength of pressed lithium hydride," *Strength of Materials*, vol. 31, pp. 625–628, Nov 1999.

[80] K. G. Rabinovich and V. K. Golubev, "Strength and fracture of lithium hydride crystals under uniaxial compression," *Strength of Materials*, vol. 31, pp. 475–478, Sep 1999.

[81] B. Buyuk, Y. Goncu, A. B. Tugrul, and N. Ay, "Swelling on neutron induced hexagonal boron nitride and hexagonal boron nitride-titanium diboride composites," *Vacuum*, vol. 177, p. 109350, 2020.

[82] D. McGregor, T. Unruh, and W. McNeil, "Thermal neutron detection with pyrolytic boron nitride," *Nuclear Instruments and Methods in Physics Research Section A: Accelerators, Spectrometers, Detectors and Associated Equipment*, vol. 591, no. 3, pp. 530–533, 2008.

[83] M. N. Mirzayev, "Heat transfer of hexagonal boron nitride (h-bn) compound up to 1 mev neutron energy: Kinetics of the release of wigner energy," *Radiation Physics and Chemistry*, vol. 180, p. 109244, 2021.

[84] E. Vance, M. Khalil, K. Pillay, H. Milledge, D. Kneff, and A. Pard, "Radiation damage in crystalline phases by (n, α) reactions," *Journal of Nuclear Materials*, vol. 108-109, pp. 726–731, 1982.

[85] F. Thévenot, "Boron carbide—a comprehensive review," *Journal of the European Ceramic Society*, vol. 6, no. 4, pp. 205–225, 1990.

[86] T. Evans, "The effects of irradiation on boron carbide. (a literature review).," 1968.

[87] C. W. Hamill and F. B. Waldrop, "Shielding studies: neutron irradiation damage to a lithium hydride compact," 1 1964.

[88] R. D. Doctor, "Radiation damage study on the lithium hydride snap shield," 10 1961.

[89] J. D. Jackson, *Classical electrodynamics; 2nd ed.* New York, NY: Wiley, 1975.

[90] Y. A. Çengel, *Thermodynamics : an engineering approach*. Sixth edition. Boston : McGraw-Hill Higher Education, [2008] ©2008, 2008. Includes bibliographical references and index.

[91] M. Paluszek, S. J. Thomas, S. A. Cohen, E. Hinterman, Y. Nagai, L. Peng, E. Ham, and G. Gaitan, *Space Nuclear Power Systems - Direct Fusion Drive*.

[92] J. Zhou and P. Bai, "A review on the methods of preparation of elemental boron," *Asia-Pacific Journal of Chemical Engineering*, vol. 10, no. 3, pp. 325–338, 2015.

[93] "Five important methods of boron carbide production," July 2021. https://www.nanotrun.com/article/five-important-methods-of-boron-carbide-production-i00108i1.html.

[94] B. Ertug, "Powder preparation, properties and industrial applications of hexagonal boron nitride," in *Sintering Applications* (B. Ertuğ, ed.), ch. 2, Rijeka: IntechOpen, 2013.

[95] L. Vel, G. Demazeau, and J. Etourneau, "Cubic boron nitride: synthesis, physicochemical properties and applications," *Materials Science and Engineering: B*, vol. 10, no. 2, pp. 149–164, 1991.

[96] K. Ma, "Synthesis of cubic boron nitride under relatively lower pressure and lower temperature via chemical reaction," *Glass Physics and Chemistry*, vol. 46, pp. 181–185, Mar 2020.

[97] C. D. Montgomery, "Fabrication and properties of lithium hydride," *Nuclear Engineering and Design*, vol. 25, no. 2, pp. 309–314, 1973.

[98] M. Antadze, G. Tsagareishvili, O. Tsagareishvili, D. Tsikaridze, and A. Khvedelidze, "Growth forms of single crystals of β-rhombohedral boron," *Journal of the Less Common Metals*, vol. 117, no. 1, pp. 153–158, 1986. Proceedings of the 8th international symposium on boron, borides, carbides, nitrides and related compounds.

[99] "What is powder metal manufacturing?," July 2021. https://llfurnace.com/blog/powder-metal-manufacturing/.

[100] R. Angers and M. Beauvy, "Hot-pressing of boron carbide," *Ceramics International*, vol. 10, no. 2, pp. 49–55, 1984.

[101] H. Wang, F. Deng, Z. Zhang, H. Xie, X. He, and H. Wang, "Study on the properties and fracture mode of pure polycrystalline cubic boron nitride with different particle sizes," *International Journal of Refractory Metals and Hard Materials*, vol. 95, p. 105446, 2021.

[102] T. Minasyan, L. Liu, S. Aydinyan, M. Antonov, and I. Hussainova, "Selective laser melting of ti/cbn composite," in *Modern Materials and Manufacturing 2019*, vol. 799 of *Key Engineering Materials*, pp. 257–262, Trans Tech Publications Ltd, 5 2019.

[103] H. Yang, H. Fang, H. Yu, Y. Chen, L. Wang, W. Jiang, Y. Wu, and J. Li, "Low temperature self-densification of high strength bulk hexagonal boron nitride," *Nature Communications*, vol. 10, p. 854, Feb 2019.

[104] "What is hot isostatic pressing (hip)?," July 2021. https://www.kobelco.co.jp/english/products/ip/technology/hip.html.

[105] A. K. Suri, C. Subramanian, J. K. Sonber, and T. S. R. C. Murthy, "Synthesis and consolidation of boron carbide: a review," *International Materials Reviews*, vol. 55, no. 1, pp. 4–40, 2010.

[106] "Hubs, a protolabs company," July 2021. https://www.hubs.com/.

[107] A. Davydova, A. Domashenkov, A. Sova, I. Movtchan, P. Bertrand, B. Desplanques, N. Peillon, S. Saunier, C. Desrayaud, S. Bucher, and C. Iacob, "Selective laser melting of boron carbide particles coated by a cobalt-based metal layer," *Journal of Materials Processing Technology*, vol. 229, pp. 361–366, 2016.

[108] H.-H. Tang and H.-C. Yen, "Slurry-based additive manufacturing of ceramic parts by selective laser burn-out," *Journal of the European Ceramic Society*, vol. 35, no. 3, pp. 981–987, 2015.

[109] R. Gheisari, H. Chamberlain, G. Chi-Tangyie, S. Zhang, A. Goulas, C.-K. Lee, T. Whittaker, D. Wang, A. Ketharam, A. Ghosh, B. Vaidhyanathan, W. Whittow, D. Cadman, Y. C. Vardaxoglou, I. M. Reaney, and D. S. Engstrøm, "Multi-material additive manufacturing of low sintering temperature bi2mo2o9 ceramics with ag floating electrodes by selective laser burnout," *Virtual and Physical Prototyping*, vol. 15, no. 2, pp. 133–147, 2020.